Design and characterization of a mobile GPR antenna assembly

A Degree Thesis
Submitted to the Faculty of the
Escola Tècnica d'Enginyeria de Telecomunicació de Barcelona
Universitat Politècnica de Catalunya
by

Albert Nadal Zaragoza

In partial fulfilment
of the requirements for the degree in
TELECOMMUNICATIONS TECHNOLOGIES AND SERVICES ENGINEERING

Advisor: Di Shi, Taimur Aftab and Alba Pagès-Zamora

Barcelona, June 2020

Abstract

Ground penetrating radars have been tested for detecting trapped alive victims from the ruins of collapsed building, for example due to a mining disaster, rock slide or natural catastrophe. The priority of the rescue teams is to find alive people as fast as they can. Rescue radars are designed with the primary objective of quickly finding survivors trapped beneath the surface.

Researchers in the Department of Microsystems Engineering (IMTEK), at the Albert-Ludwigs University of Freiburg, have been working on experiments about antenna designing and measuring systems for rescue radar through the years. Currently, IMTEK is working in a project which objective is to develop a sensor system for the localization of buried people. This thesis has been developed there, that is why it is focused on their needs and possibilities.

The aim of the thesis is to develop a mobile GPR antenna assembly which can be used as a rescue radar. The project is composed of three fundamental parts: different kinds of HF-simulations software for GPR applications comparison, while verifying if MATLAB openEMS open free source can be used for designing antennas in IMTEK department projects; designing and optimizing the GPR antenna assembly while analyzing different techniques for crosstalk isolation enhancement such us adding rings, meander-line and Electromagnetic Band Gap; and once the prototype is defined and manufactured, testing the GPR antenna in different scenarios.

As a conclusion of the work, the simulations results of both software used were very close from the antenna prototype datasheet diagrams as well as from the experimental tests did. Therefore, Matlab openEMS software has also proved to be very competent in antenna designing sector, obtaining practically identical results as the CST Studio Suit software. Furthermore, after analyzing the performance of different GPR antenna modifications and the isolation enhancement structures added to the design, we concluded that the Electromagnetic Band Gap technique with square sides equal to 15 mm is the best isolation enhancement, therefore, we manufactured and tested a replica of the GPR antenna design with EBG structure.

Resum

Els georadars han estat provats per detectar víctimes vives atrapades a les ruïnes d'edificis esfondrats per diverses causes, com desastres en una mina, despreniments de roques o catàstrofes naturals. En aquests casos, la prioritat dels equips de rescat és trobar els supervivents atrapats sota la superfície el més ràpid possible.

Els radars de rescat estan dissenyats amb l'objectiu principal de satisfer aquesta necessitat. Durant els darrers anys, investigadors del Departament d'Enginyeria de Microsistemes (IMTEK) de la Universitat Albert-Ludwigs de Friburg han realitzat experiments i investigacions sobre antenes i sistemes de mesura per a radars de rescat. Actualment, l'IMTEK treballa en un projecte enfocat a desenvolupar sistemes amb sensors incorporats per a la localització de persones enterrades sota la superfície. La present tesi, realitzada en aquest departament, es centra en les seves necessitats i possibilitats.

L'objectiu principal d'aquesta tesi és desenvolupar un georadar mòbil amb aplicació directa als radars de rescat. El treball està compost per tres parts principals: comparar diferents tipus de programaris de simulació HF per a aplicacions de georadars, mentre al mateix temps verificar si el software obert MATLAB openEMS pot ser útil per dissenyar antenes en els projectes del departament IMTEK; dissenyar i optimitzar el muntatge del georadar mentre s'analitzen diferents tècniques d'isolació de la comunicació creuada i, en darrer lloc, quan el prototip estigui definit i fabricat, realitzar diferents proves d'escenaris específics per a georadars.

Els resultats obtinguts pels dos programes de simulació emprats en el projecte van ser molt similars al *datasheet* de l'antena utilitzada i als experiments efectuats. Per tant, es pot concloure que MATLAB openEMS és igual de competent que el software CST Studio Suit en el sector del disseny d'antenes. Finalment, després d'analitzar el desenvolupament de les diferents modificacions fetes al georadar i afegir diferents tècniques d'isolació, l'estructura de bandes electròniques quadrades de costat 15 mm va presentar els millors resultats, de manera que es va manufacturar i testejar una rèplica del georadar incorporant l'estructura de bandes electròniques.

Resumen

Los georadares se han probado para detectar víctimas atrapadas en las ruinas de edificios derrumbados por causas diversas, como desastres en una mina, desprendimientos de rocas o catástrofes naturales. En estos casos, la prioridad de los equipos de rescate es encontrar los supervivientes atrapados debajo de la superficie lo más rápido posible.

Los radares de rescate están diseñados con el objetivo principal de satisfacer esta necesidad. Durante los últimos años, investigadores del Departamento de Ingeniería de Microsistemas (IMTEK) de la Universidad Albert-Ludwigs de Friburg han realizado experimentos e investigaciones sobre antenas y sistemas de medida para radares de rescate. Actualmente, el IMTEK trabaja en un proyecto enfocado a desarrollar sistemas con sensores incorporados para la localización de personas enterradas debajo de la superficie. La presente tesis, realizada en este departamento, se centra en las necesidades y posibilidades.

El objetivo principal de esta tesis es desarrollar un georadar móvil con aplicación directa a los radares de rescate. El trabajo está compuesto por tres partes principales: comparar diferentes tipos de programas de simulación HF para aplicaciones de georadares, mientras al mismo tiempo verificar si el software gratuito MATLAB open EMS puede ser útil para diseñar antenas en los proyectos de departamento IMTEK; diseñar y optimizar el montaje del georadar mientras se analizan diferentes técnicas de aislamiento de la comunicación cruzada y, en último lugar, cuando el prototipo este definido y fabricado, realizar diferentes pruebas de escenarios específicos para georadares.

Los resultados obtenidos por los dos programas de simulación empleados en el proyecto fueron muy similares al *datasheet* de la antena utilizada y a los experimentos realizados. Por tanto, se puede concluir que MATLAB openEMS es igual de competente que el software CST Studio Suit en el sector del diseño de antenas. Finalmente, después de analizar el desarrollo de las diferentes modificaciones realizadas al georadar y añadir diferentes técnicas de aislamiento, la estructura de bandas electrónicas cuadradas de lado 15 mm presentó los mejores resultados, de manera que se manufacturó y testeó una réplica del georadar incorporando la estructura de bandas eléctricas.

Acknowledgements

Firstly, I would like to thank the support given by my advisors in Freiburg, Di Shi and Taimur Aftab. They provided me the necessary knowledge at the beginning and during the thesis. Also, they dedicated a lot of time and effort for being in touch with me and despite the current situation difficulties I lacked for nothing. I have to recognize that the correct development of my Bachelor's thesis in part was thanks to their dedication.

Secondly, apart from the help and the accurate follow-up of the project I have received from my supervisors in Freiburg, I would like to especially thank the opportunity that Professor Leonhard Reindl has been given me to take part of this project. Needless to say, the Professor has also contributed to the initial idea of the thesis and he supervised my thesis work as well.

Moreover, I would like to be thankful to all the technical and secretary staff of IMTEK for helping me with anything I needed as well as providing me all the material for the good development of my thesis.

Last, but not least, I also thank my Barcelona's supervisor, Alba Pagès-Zamora for the guidance and encouragement in finishing this project. It was a great comfort and relief to know that she was willing to provide me all I needed. I am really grateful for affording me this enriching and wonderful opportunity.

Revision history and approval record

Revision	Date	Purpose
0	04/05/2020	Document creation
1	13/06/2020	Document revision

DOCUMENT DISTRIBUTION LIST

Name	e-mail
Albert Nadal	Albert4.nadal@gmail.com
Di Shi	di.shi@imtek.de
Taimur Aftab	aftab@imtek.de
Alba Pagès-Zamora	alba.pages@upc.edu

Written by:		Reviewed and approved by:	
Date	29/06/2020	Date	29/06/2020
Name	Albert Nadal	Name	Di Shi
Position	Project Author	Position	Project Supervisor

Table of contents

List of Figures

List of Tables:

Glossary

EBG: Electromagnetic Band Gap

EM: Electromagnetic

FDTD: Finite-Difference Time-Domain method

FOUNT$_2$: Fliegendes Lokalisierungssystem für die Rettung und Bergung von Verschütteten (Flying localization system for searching and rescuing buried people). Second project started with the same name.

GPR: Ground Penetrating Radars

HF: High Frequency

IMTEK: Institut für Mikrosystemtechnik (Deparment of Microsystems Engineering)

i-LOV: Intelligentes Sicherndes Lokalisierungssystem für die Rettung und Bergung von Verschütteten (Intelligent secure localization system for rescuing buried people)

PML: Perfect Matched Layer

RF: Radio Frequency

SORTIE: Sensor Systeme zur Lokalisierung von verschütteten Personen in ein-gestürzten Gebäuden (Sensor Systems for Localization of Trapped Victims)

UAV: Unmanned Arial Vehicle

WP: Work Package

1. Introduction

1.1. Statement of Purpose

The purpose of this project is to design and characterize a mobile GPR (Ground Penetrating Radar) antenna assembly. This assembly will be part of a mobile GPR node deployed by an UAV (Unmanned Arial Vehicle) on top of buildings, which collapsed due to catastrophe like earthquake, for detecting and localizing buried alive people. The main objective is detecting trapped alive victims from the ruins of collapsed building, the living person could be detected by the bioradar thanks to the RF-Doppler shift caused by the chest movement due to breathing.

The whole SORTIE (Sensor systems for the localization of buried people in collapsed building) system is illustrated in Figure 1.1(a). These nodes will be released from the UAV system at the desired detecting place.

The bioradar node system is made up of a radar-board, a mother-board, a Transmission antenna (Tx) and Receiving antenna (Rx) system for detecting people, an antenna to establish communication between the node and the UAV and a battery. The GPR node is represented in Figure 1.1.(b). Also, the two antenna abovementioned, which design, the thesis consists of are shown at the bottom of the Figure 1.1.(b):

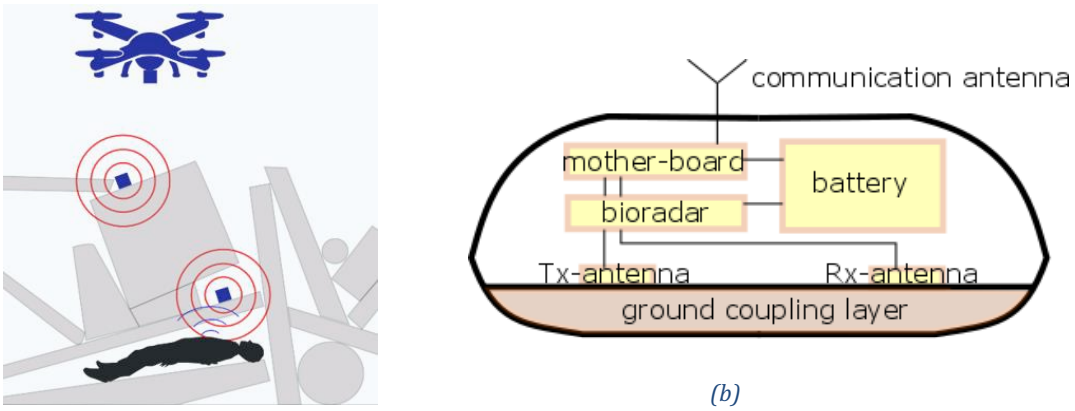

(a) *(b)*

Figure 1.1: a) Platform for detecting trapped victims, b) construction concept of the SORTIE-Bio radar system.

The main objectives of the project are the following ones: different kinds of HF-simulations software for GPR applications comparison, while verifying if MATLAB openEMS open free source can be used for designing antennas in IMTEK department projects; designing and optimizing the GPR antenna assembly while analysing different techniques for crosstalk isolation enhancement such as adding rings, meander-line and Electromagnetic Band Gap; and once the prototype was defined and manufactured, testing the GPR antenna in different scenarios.

1.2. Requirements and Specifications

Project requirements:

- The author should plan and execute the project systematically.
- The author should be able to learn the related knowledge and analyze the simulation and experimental results.

- The author should be able to write scientific report and give scientific presentation.

Project specifications:

- The author should carry out reasonable results according to the work plan.

1.3. Methods and Procedures

Recently, IMTEK has been awarded a German federally funded project called SORTIE. Within this project an aerially deployable bioradar sensor node will be developed. IMTEK has collected a lot of research and development experience on bioradar from former related projects like i-LOV and FOUNT2.

The research project SORTIE is a continuation from the project FOUNT2. However, this bachelor thesis project is started from scratch.

This bachelor project is being supervised by the Professor Leonhard Reindl and his Ph.D. students Di Shi and Taimur Aftab.

On account of the current pandemic situation, I worked the first month at the University Laboratory and from middle March to middle of June the thesis has been done while working from home. Soon after having taken up the thesis, we dismissed all the on-site working. However, this did not mean a setback in terms of communications with my supervisors, we kept doing at least one video call meeting per week. Lastly, we just went to the University when we wanted to do the experimental tests of the antenna assembly. The tests have been done in the RF laboratory at the IMTEK facilities, under the supervision of my supervisors.

1.4. Work Plan

The work plan consists of the following work packages:

WP1 (From 18/02/2020 to 07/04/2020) - Simulation software comparison: Compare different types of software simulations results with same design modifications**.**

- Internal task T1: **Setup of tools**
- Internal task T2: **Numerical experiments**
- Internal task T3: **Results analysis**

WP2 (From 23/03/2020 to 22/05/2020) - Design of a bi-static GPR antenna module: Design and manufacture the final bi-static GPR antenna module prototype

- Internal task T1: **Geometric design**
- Internal task T2: **Parametric sweep**
- Internal task T3: **Results post processing**
- Internal task T4: **Design of impedance transformation network** (No enough time)
- Internal task T5: **Porting the design to a circuit layout tool**
- Internal task T6: **Fabrication of the antenna module**

WP3 (From 14/05/2020 to 29/05/2020) - Experimental validation: Carry out different experimental tests with the final manufactured prototype

- Internal task T1: **Ground penetration transmission test** (Add results in final presentation)
- Internal task T2: **Ground penetration transmission test for a setup with breathing robot** (No enough time)
- Internal task T3: **Results post processing**

WP4 (From 16/05/2020 to 24/05/2020) - Documentation and writing: Fill in all the documentation

- Internal task T1: **Documentation and thesis deliverables**

Throughout the project the Gantt diagram has changed due to the incidences and delays. Therefore, two different Gantt were defined, one at the beginning of the thesis (Figure 1.2(a)) and another one redefined roughly at the mid of the project after the incidences (Figure 1.2(b)).

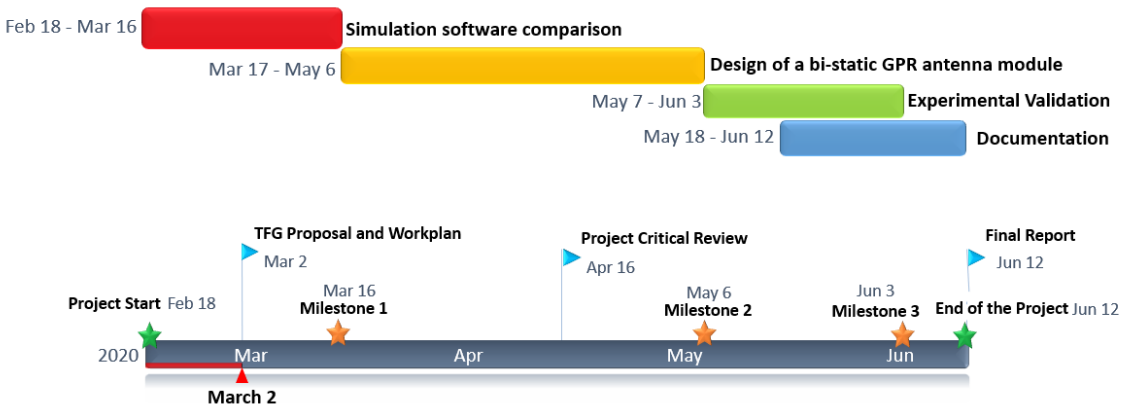

(a)

Each work package has a different colour: **WP1**, **WP2**, **WP3** and **WP4**.

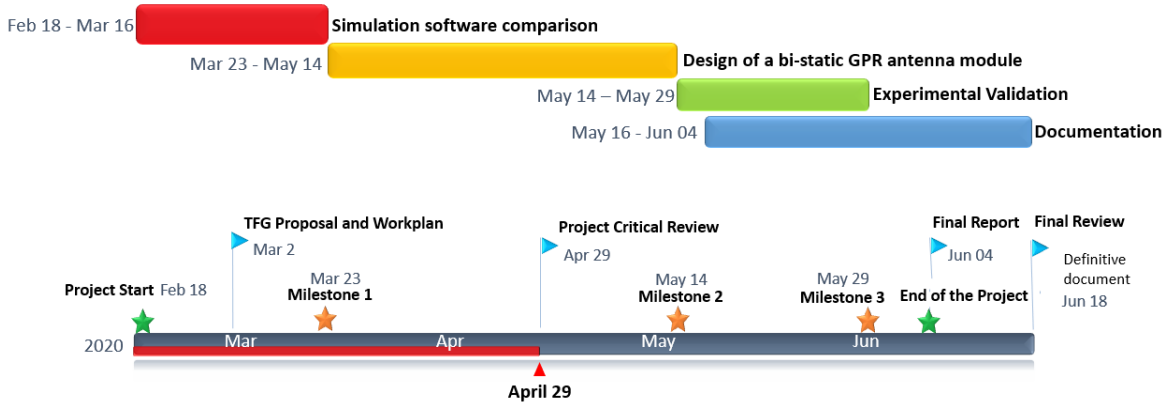

(b)

Figure 1.2: Gantt diagram representation throughout the project: a) work plan diagram, b) critical review diagram.

There was also a time delay concerning the milestones defined at the beginning. As presented in the following Table 1.1, I have only added the last milestones modified:

WP#	Task#	Short title	Milestone / deliverable	Date (week)
1	**T2-T3**	Design improvements	Results analysis done	23/03/2020
2	**T8**	Final design prototype	Fabrication of the antenna module done	14/05/2020
3	**T3**	Experimental validation	Experimental tests done	29/05/2020

Table 1.1: Milestone deadlines.

1.5. Incidences and modifications

I had to do an adjustment of my working place and conditions and this implied a time delay. After analysing very carefully the situation, we realized that much work remained to be done, not only because of the COVID-19 crisis but also because the Project proposal and Work plan might be a little bit oversized.

Still we tried to complete all the tasks initially proposed. There were not big changes compared to the task structure defined at the beginning of the thesis.

Regarding the WP1 and WP2, as said, a time delay was experienced due to the corona virus pandemic, which implied that the planned dates of several sub work packages were delayed.

However, I have started WP4 ahead of schedule, which made the work better organized and saved a bit time for the delayed work packages.

Additionally, the WP-2 internal task T7: “Fabrication of the antenna module’’ will be outsourced to the university workshop or a company.

Finally, it was impossible to accomplish the task 4 of WP2 and the task 2 of WP3. The big amount of time taken to conclude the best performance for the GPR antenna assembly, prevents us from doing the impedance transformation network and some experimental tests. But being conscious of the importance of it, even though the impedance matching network and the antenna GPR experimantal tests were not added at the thesis report, it might be included at the final presentation.

2. State of the art of the technology used or applied in this thesis:

2.1. Ground Penetrating Radars (GPR)

GPR is a geophysical survey method that uses pulses of electromagnetic radiation to image the subsurface. GPR systems consist of transmitting and receiving antenna, a power source connected to the transmitting antenna and methods of signal processing equipment added at the receiving antenna [1]. The antenna characteristics, the choice of the transmitted signal and the post processing methods depend on the application for the GPR system.

GPR systems are used in the detection of objects buried under the earth's surface, for example, piping, cables, hidden tunnels and underground mines [2].

GPR is mainly used to provide information of geographical exploration, but currently, it has also begun to be a technology for detecting trapped alive victims. In fact, all this thesis research will be mainly determined by this application field.

2.1.1. GPR application for detecting trapped alive victims

GPR has been tested for detecting trapped alive victims from the ruins of building collapsed, for example due to a mining disaster, rock slide or natural catastrophe. The priority of the rescue teams is to find alive people. Rescue radars are designed to quickly find survivors trapped beneath the surface.

Many techniques are being applied for detecting trapped people such as micro-cameras and high sensitivity microphones. But the problem is the low penetration depth provided [3]. Therefore, many researching groups have started studying the option to use ground penetrating radar as a solution to penetration depth issue.

IMTEK has also been working in this application field for a long time. In Figure 2.1 is shown different platform types with GPR incorporated for detecting trapped victims. The design of platform 3 is the final objective of this thesis.

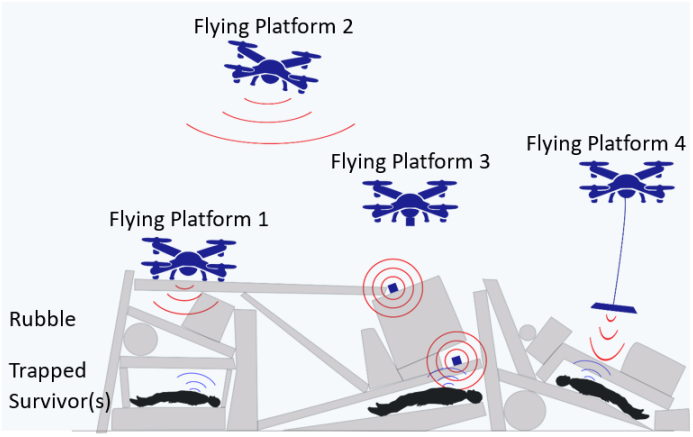

Figure 2.1: Different platform types for detecting trapped victims.

2.2. GPR main features

Over the last several decades, GPR researching usually used a radar with a frequency under 1GHz [4], because the lower the frequency is, the more penetration depth the radar can achieve. However, many research groups are starting to analyze the performance of the radar with higher frequency.

The following is a more detailed explanation of which factors have to be taken into account before deciding the radar frequency.

The exploration depth and the radar range resolution are the most important parameters to take into account before deciding an appropiate GPR antenna [5]. The performance of the antenna will be controlled by the tradeoff between these two parameters. As Figure 2.2, the exploration depth is the maximum distance which the radar can detect a target and the range resolution (ΔR) indicates the ability of the radar to identify closely spaced targets.

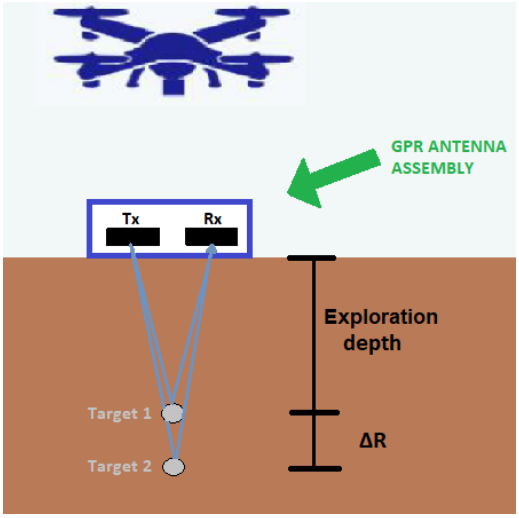

Figure 2.2: Graphic representation of the most important parameters in antenna frequency choice.

2.2.1. Exploration depth

The exploration depth depends on many factors such as the ground material characteristics (the radar waves depth penetration progressively decreases as the conductivity of a material increase), scattering losses and the GPR frequency.

The antenna power P at some other point z is related to P_0 (P at $z = 0$) [6] as follows

$$P(z) = P_0 e^{-2\alpha_c z} \tag{2.1}$$

where α_c is the ohmic attenuation coefficient and depends on the material and frequency, higher frequencies attenuate more rapidly [7].

Analysing the Eq. (2.1) above, the lower GPR antenna frequency you choose, the less attenuation the radar will suffer. And the lower is the attenuation, the more power the antenna will have and consequently the exploration depth increases as well.

2.2.2. Range resolution

Regarding the range resolution, it depends on the operating bandwidth BW of the radar as it can be seen at the formula below [8]

$$\Delta R = \frac{c}{2 \cdot BW} \tag{2.2}$$

where $\boldsymbol{c}$ is speed of light in medium

$$c = \frac{c_0}{\sqrt{\mu_r \cdot \epsilon_r}} \tag{2.3}$$

and c_0 is speed of light in vacuum.

Eq. (2.2) and (2.3) show that as the bandwidth of the radar increases, the range resolution (ΔR) decreases. Therefore, it is possible to distinguish two closer targets which means that the resolution is better.

Furthermore, for one kind of antenna design, if the antenna's dimensions are proportionally scaled, the fraction bandwidth remains almost the same. Therefore, the higher the resonance frequency, the bigger is the absolute bandwidth.

Summarizing the information above, increasing the GPR antenna frequency improves the GPR range resolution.

2.2.3. GPR frequency decision

Prioritizing between the exploration depth and range resolution has always been the most critical decision when calculating the main GPR features. This decision is directly related to the choice of radar frequency, because whether the depth is prioritized, it must be chosen a low frequency. However, when the radar resolution is prioritized, the frequency must be higher.

Even if it is more common to work with a frequency lower than 1GHz because it can provide more exploration depth, we decided to use a ceramic patch antenna prototype with central frequency at 2.45 GHz with the aim of verifying if we could also obtain enough exploration depth and resolute experimental results with it.

The antenna prototype's main advantages for the designed GPR node are the following ones: using high frequencies the antenna prototype is quite small and with light weighs, therefore, it will be easier to introduce it within the drone; with 2.4GHz antenna, there are much more researching and availability in the market and you can obtain it for low costs; it has been a priority to obtain good resolution in order to clearly distinguish between people and not interested objects.

3. Methodology / project development:

This section includes information on the mathematical method used by the software; it gives a brief overview of each software used and how they work; it also contains a description and some features details of the chosen antenna prototype; finally, an introduction of the structures for isolation enhancement tested in this thesis is done.

3.1. Mathematical modelling

3.1.1. Finite-Difference Time-Domain method (FDTD)

The Finite-Difference Time-Domain (FDTD) solves Maxwell's equations in the time domain using finite-difference approximations.

To resolve electromagnetic problems, the idea is to simply discretize the Maxwell's equations in time and space with central difference approximations [9].

Maxwell's equations for an isotropic, time-invariant and homogeneous medium are:

$$\nabla \times \boldsymbol{E} = -\mu \frac{\partial \boldsymbol{H}}{\partial t} \longrightarrow \frac{\partial \boldsymbol{H}}{\partial t} = -\frac{1}{\mu} \nabla \times \boldsymbol{E} \tag{3.1}$$

$$\nabla \times \boldsymbol{H} = -\varepsilon \frac{\partial \boldsymbol{E}}{\partial t} \longrightarrow \frac{\partial \boldsymbol{E}}{\partial t} = \frac{1}{\varepsilon} \nabla \times \boldsymbol{H} \tag{3.2}$$

where ε is the permittivity, μ is the permeability, **E** is the electric field vector and **H** the magnetic field vector. Then, the FDTD method approximates the derivatives of Maxwell's Equations with the following finite-difference:

$$\frac{\partial \boldsymbol{H}}{\partial t} = -\frac{1}{\mu} \nabla \times \boldsymbol{E} \longrightarrow \frac{\boldsymbol{H}\left(t + \frac{\Delta t}{2}\right) - \boldsymbol{H}\left(t - \frac{\Delta t}{2}\right)}{\Delta t} = -\frac{1}{\mu} \nabla \times \boldsymbol{E}(t) \tag{3.3}$$

$$\frac{\partial \boldsymbol{H}}{\partial t} = \frac{1}{\varepsilon} \nabla \times \boldsymbol{H} \longrightarrow \frac{\boldsymbol{E}(t + \Delta t) - \boldsymbol{E}(t)}{\Delta t} = \frac{1}{\varepsilon} \nabla \times \boldsymbol{H}(t + \frac{\Delta t}{2}) \tag{3.4}$$

where Δt is the time step, which will be much less than the frequency of interest. In addition, for stability reasons, a field component cannot propagate more than the space resolution, this means that a common choice for Δt (in one, two- or three-dimension problems) is given by [9]:

$$\Delta t = \frac{\Delta}{2 \cdot c_0} \tag{3.5}$$

where Δ is the resolution of the different axis.

In FDTD simulations, the space is divided into small cells. There are assigned different points on the surface of the cells and each surface cell point should satisfy Maxwell's equations. Thus, electromagnetic waves are simulated to propagate for the whole space needed, almost equal as they do in real physical situation. The basic algorithm of FDTD was defined by K.S. Yee in 1966, [10].

Our interest is focused in three-dimensional FDTD solver. The formulation in 3D case is based on discretizing the volume domain with a regular rectangular grid [11]. As shown in Figure 3.1, each grid cell has dimensions Δx, Δy and Δz along each Cartesian axis and there are six approximated differential equations, one for each electromagnetic field component: Ex, Ey, Ez and Hx, Hy, Hz.

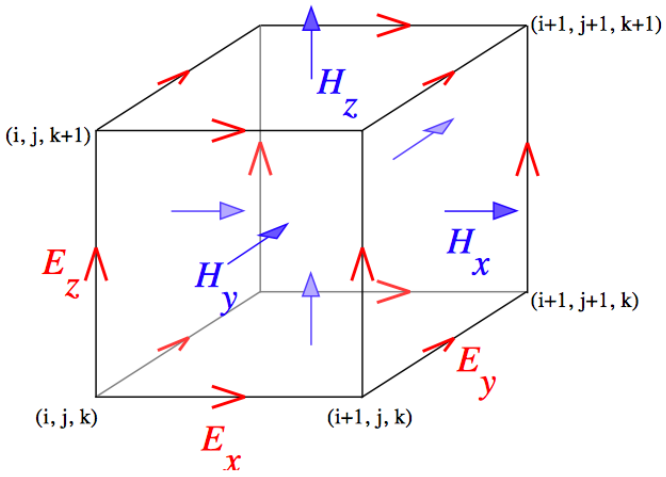

Figure 3.1: The Yee cell used in FDTD method [10].

3.1.2. Boundary condition: Perfectly Matched Layer (PML)

Because the FDTD is a method that uses differential equations, the boundary conditions must be specified. For GPR antenna applications, the boundary conditions must be like a PML in order to simulate a free space scenario.

PML absorbing boundary conditions are designed to absorb incident electromagnetic waves with minimal reflections [12].

3.2. FDTD Software

For the software development two different kind of software were used, namely CST Studio Suite with a student license and MATLAB openEMS. In both software we used time solvers that are based on FDTD method.

These software tools are very complete for designing 3D antennas, postprocessing the simulation results and analyzing the performance of antenna.

They both complement each other very well. The limitations on the design size of CST Studio Suit student license were compensated with MATLAB openEMS, whereas the MATLAB openEMS difficulty for doing fast parameter sweeps of the antenna dimensions was covered with the rapidity and efficiency of CST software.

3.2.1. CST Studio Suite

CST Studio Suite is a high-performance 3D EM analysis software for designing, analyzing and optimizing electromagnetic components and systems. With CST, it is possible to choose between different powerful solver modules and boundaries conditions.

We proceed using the time domain solver, which is a 3D full-wave solver that implements finite integration techniques. The time domain solver can perform broadband simulations in a single run. This solver is efficient for most kinds of high frequency applications such as connectors, transmission lines, filters and antennas [13].

In CST Studio Suite when you enter the boundaries properties, the design modeled structure is surrounded by a bounding box. This box is built with the different boundaries that you have previously defined for each box face. The boundaries which fit best for our antenna design was the Open (add space) type.

The Open (add space) extends the touching geometry virtually to infinity by using a PML as a boundary. Also, it adds some extra space between the antenna structure and the applied boundaries conditions.

CST Studio Suite has a wide variety of geometric figures to add as well as different kinds of power supplies.

The procedure to do the antenna design was the following one: firstly, a parameter list with all the components dimensions was added; secondly, the antenna and the coaxial feeder were defined; finally, a waveguide port at the bottom part of the coaxial connector for feeding the antenna was incorporated.

3.2.2. MATLAB openEMS

MATLAB openEMS is a free and open electromagnetic field solver which use FDTD method. It supports Cartesian and cylindrical coordinates system.

Regarding the definition of the boundary conditions used with this software, there was the option of Perfectly Matched Layer (PML) using an artificial “x” numbers of cells thick layer which absorbs the incoming electromagnetic waves.

The procedure to do the antenna design was the following one. To start with, it was indispensable to have a look at the different tutorial codes that were available on openEMS website. Then, the code for creating step by step the antenna design was made. In this case, the software was not as intuitive as CST Studio Suit, with MATLAB openEMS, you define all the components shapes and dimensions programming with different functions.

3.3. Antenna starting-point

After introducing the principal parameters for designing the GPR antenna and the frequency selected for this project, an in-depth analysis of the chosen antenna prototype is given in the next section.

3.3.1. Antenna prototype description

The mobile GPR antenna assembly will be made using two equal antenna prototypes. The antenna prototype is a ceramic patch with central frequency at 2.450 GHz. Figure 3.2 is extracted from the antenna prototype datasheet [14] and shows a photo of the antenna and a design plan with its dimensions.

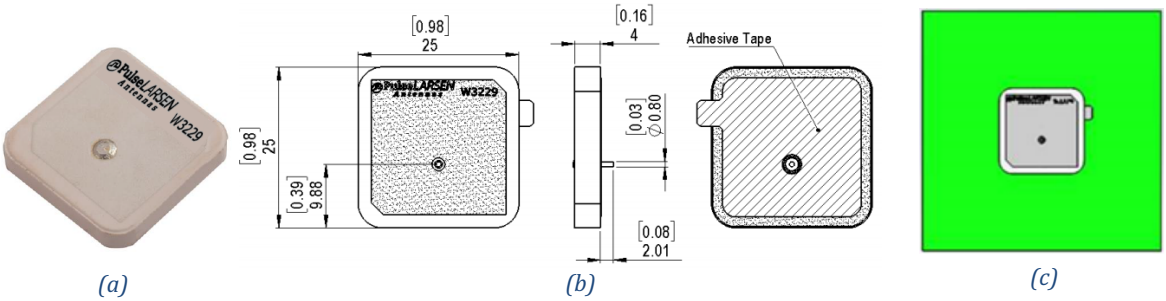

Figure 3.2: Antenna prototype [14]: a) real antenna, b) design plan, c) real antenna with ground plane.

The antenna consists basically of four different component: a metal ground plane as bottom layer; in the middle of the antenna, there is a dielectric ceramic substrate; as a top layer a metalic patch; lastly, the antenna also has a copper and tinplated pin for feeding the antenna.

The component dimensions are specified in the table 3.1 [14]:

Component	**Dimensions**
Metalic ground plane	70x70x0.075 mm
Ceramic Substrate	25x25x4 mm
Metalic patch	21x21x0.075 mm
Pin	Length= 0.08mm; Ø= 0.03mm

Table 3.1: Antenna Prototype component dimensions.

The main features and the behaviour charts of the antenna are the following ones [14]:

Frequency range	2400-2500 MHz
Size	25x25x4 mm
Polarization	RHCP
Gain	+6.5 dB
Feed	Pin feed, adhesive tape
Moisture sensitivity level	MSL1

Table 3.2: Antenna prototype features.

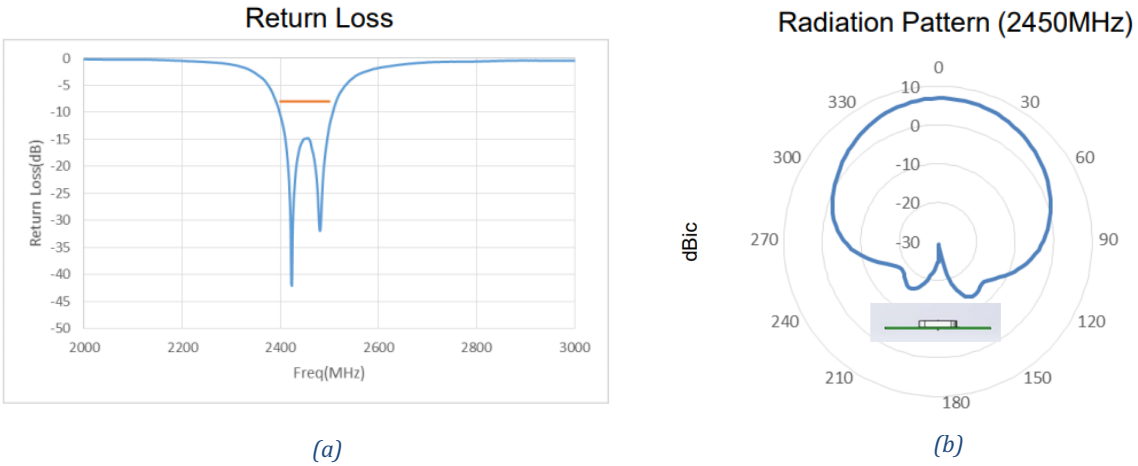

(a) *(b)*

Figure 3.3: a) Antenna's return loss chart, b) antenna's 2D radiation pattern.

In Figure 3.3 (a), the antenna has two resonance peaks between 2.4 and 2.5 GHz and an approximate bandwidth of 1GHz. Moreover, Figure 3.4 (b) shows that the ceramic patch antenna radiation pattern has a big main lobe of 6.5 dBi.

3.3.1.1. Antenna prototype analysis of main design characteristics

After explaining the main features of the antenna prototype, an analysis of the antenna prototype main design peculiarities such us the trimmed corners and the feeding point is done.

At the end of the circular polarized antenna section of the Balanis book [6] is shown that if the ends of two opposite corners of a square patch antenna are trimmed, circular polarization can be achieved.

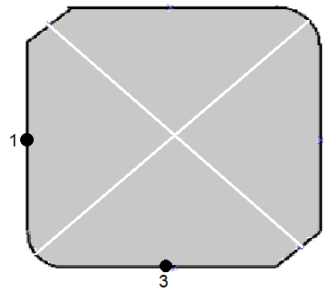

Figure 3.4: Replica of Balanis book image from the circular polarization section of microstrip antenna.

Also, [6] specifies that the feeding point must be placed at the point 1 or 3 of the Figure 3.5 in order to radiate two orthogonal field components with equal amplitude and in phase quadrate, therefore, the patch design achieve the circular polarization. The antenna prototype chose for this thesis has the feeding point placed at point 3 of the Figure above in order to have circular polarization.

The study did in [15] is a detailed analysis of different single feed circularly polarized microstrip antennas similar to our antenna prototype. From the document, it can be concluded that the trimmed corners also provide a notable improvement of the antenna bandwidth.

In the results section, the theoretical information read in the documents, it will be verified with our own CST and MATLAB open EMS antenna design.

3.4. GPR antenna assembly components

Apart from the antenna prototypes Tx-antenna and the Rx-antenna used for the GPR antenna assembly design, it is also needed a coaxial connector that fits for the frequency range of 2.4-2.5GHz. Therefore, an SMA coaxial connector and RG174 cable is chosen for feeding the antenna.

3.5. GPR antenna assembly isolation techniques employed

After designing the GPR antenna assembly and analyzing the best characteristics for the antenna, different isolation techniques are added in order to check whether there might be significant isolation enhancement.

The techniques of isolation enhancement analyzed are: rings, meander-line and Electromagnetic Band Gap (EBG).

First of all, the idea of adding rings around the two antennas is the simplest way for isolation enhancement. In a recent paper [16], a ring structure for isolation improvement is presented.

Secondly, from paper [17], a slotted meander-line resonator was implemented and evaluated.

Finally, different kinds of EBG structures for isolation enhancement were tested. We estimated the structure dimensions which would fit for our frequency range [18] and [19].

Figure 3.5 corresponds to the different isolation structures above:

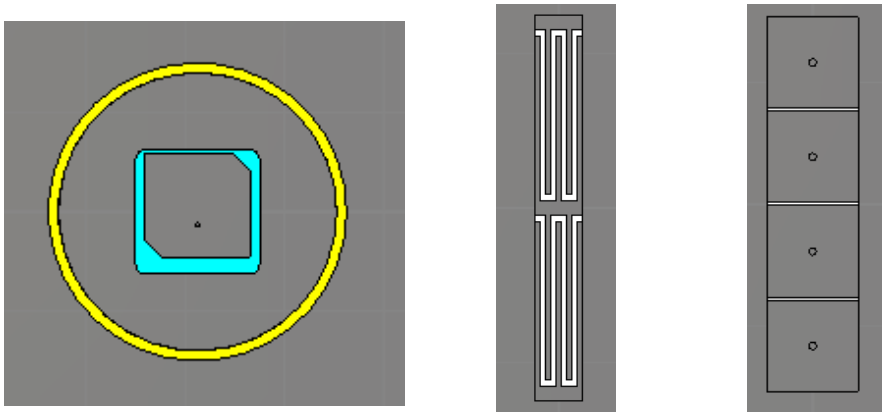

(a) (b) (c)

Figure 3.5: Isolation techniques: a) ring, b) meander Line, c) electromagnetic band gap.

4. Results

The results section shows all the simulation analysis and experimental tests done towards the objective of designing a GPR antenna assembly. Firstly, one of the GPR antennas following the prototype mentioned in section 3.4.1 was designed. Secondly, an analysis and experimental tests of the final antenna were done; Finally, to design and figure out the optimal GPR antenna, different design modifications and isolation structures were tried.

4.1. Comparison between CST Studio Suite and MATLAB openEMS

The objectives in this section were to replicate one antenna prototype with CST and MATLAB openEMS analyzing the different antenna characteristics step by step; once the antenna design replica was finished, a comparison between both software was done. It was proven that MATLAB openEMS can be as good as CST is in antenna designing.

4.1.1. Antenna ceramic substrate, relative permittivity analysis and definition

The antenna prototype datasheet does not give information about the ceramic substrate properties. Therefore, the substrate relative permittivity value was found out doing some simulations of a basic replica design of the antenna prototype. As shown in Figure 4.1, the first parameter sweep was from 2 to 10 with step width of 1:

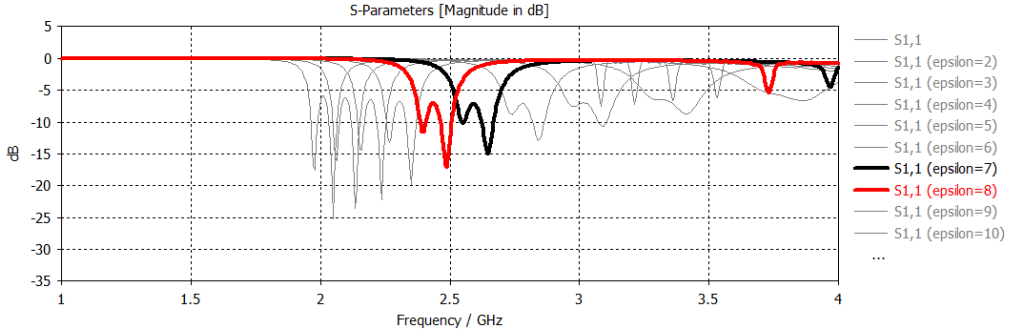

Figure 4.1: Relative permittivity definition - first parameter sweep of the A from 2 to 10; S11 parameter antenna chart.

Figure 4.1 shows the return loss values in dB of the first antenna design replica. At that time, the return loss values were not important because the antenna design was not the final one, many changes in antenna design were still needed. The analysis was focused on where the antenna resonance peaks were placed. Compared with the return loss of the antenna prototype datasheet (Figure 3.4 (a)), the interested frequency range is from 2.4GHz to 2.5GHz, therefore, analyzing the results, the closest S11 parameter shape with respect to the antenna data sheet were between the epsilon values from 7 and 8. In order to obtain more accurate relative permittivity value, a second parameter sweep was done from 7.25 to 8.75 with step width of 0.25:

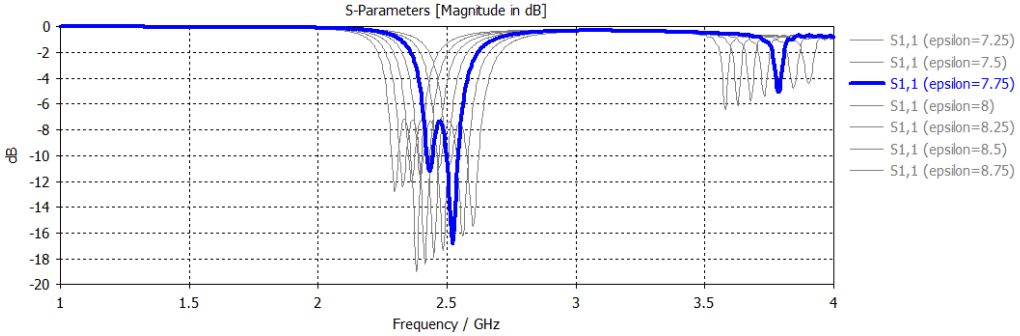

Figure 4.2: Relative permittivity definition – second parameter sweep from 7.25 to 8.75; S11 parameter antenna chart.

Comparing again with the return loss data sheet chart of the antenna prototype, the most similar resonance peaks place is obtained with ceramic substrate material (epsilon) value equals to 7.75. Therefore, we use this value for further simulations.

4.1.2. Antenna design features and different design changes

Table 4.1 presents the different materials characteristic and dimensions of all the components used for the antenna design simulations in both software:

Ground Plane	PEC (Perfect electrical conductor) **- 70x70x0mm**
Substrate	Ceramic (**Epsilon** = 7.75; **Mu** = 1) **- 25x25x4mm**
Patch	PEC (Perfect electrical conductor) **- 25x25x4mm**
Ring (Step 6)	Aluminum (**Epsilon** =2.53; **Mu** = 1; **Density** = 1550 kg/m^3) **- Width= 1mm; ø = 50mm**
Ground Box (Step 7)	Sandy Soil: dry (**Epsilon** = 10^{-12}; **Mu** = 1; **Density** = 2700 kg/m^3) **- 250x250x250mm**
Ground Box (Step 8)	Concrete: one year old (**Epsilon** = 1; **Mu** = 1; **Density** = 2400 kg/m^3) **- 250x250x250mm**

Table 4.1: Antenna design materials.

The design evolution from simple patch antenna to the antenna prototype replica was done below. The following design changes have been strictly followed and analyzed one by one:

1. Square patch on a square substrate with coaxial feed
2. Cut-corners patch on a square substrate with coaxial feed
3. Cut-corners patch on a smoothened square substrate with coaxial feed
4. Same as (3), shifting the patch
5. Same as (4), with cylindrical ground plane
6. Same as (5), with a metal ring around the patch
7. Same as (5), adding a ground box of Sandy Soil
8. Same as (5), adding a ground box of Concrete

1- Square patch on a square substrate with coaxial feed

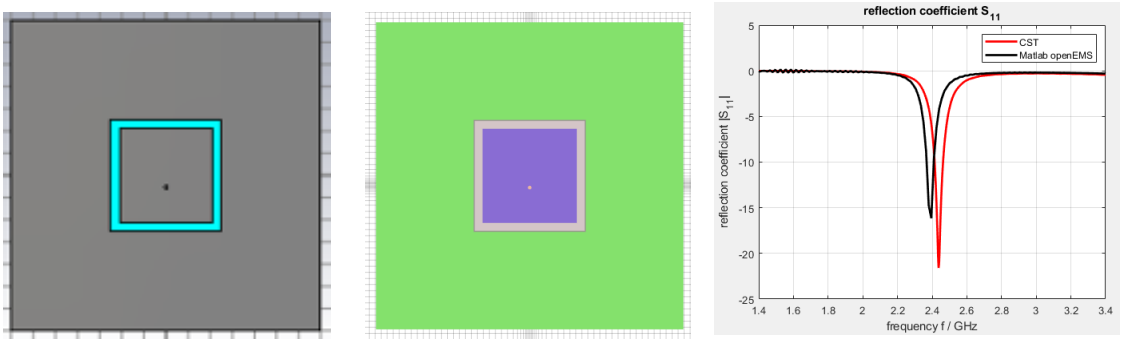

(a) (b) (c)

Figure 4.3: Step 1: a) CST studio suit design, b) MATLAB openEMS design, c) S11 parameter – comparison between both software.

2- Cut-corners patch on a square substrate with coaxial feed

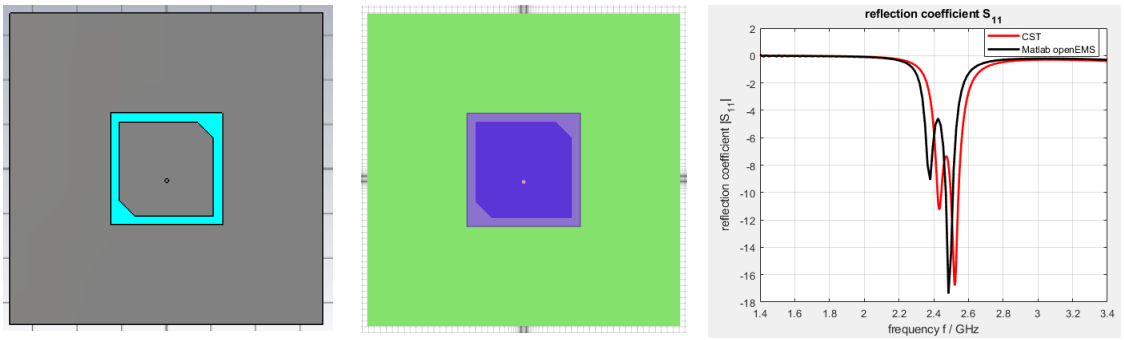

(a) *(b)* *(c)*

Figure 4.4: Step 2: a) CST studio suit design, b) MATLAB openEMS design, c) S11 parameter – comparison between both software.

Step 1 to 2 analysis: Cutting the corners caused a big change regarding the S-parameters, the design has in step 1 one peak at 2.5GHz, now it has two resonance peaks in the desired frequency interval (from 2.4 to 2.5 GHz). Apart from the change in S11 shape, the antennas bandwidth increased considerably.

3- Cut-corners patch on a smoothened square substrate with coaxial feed

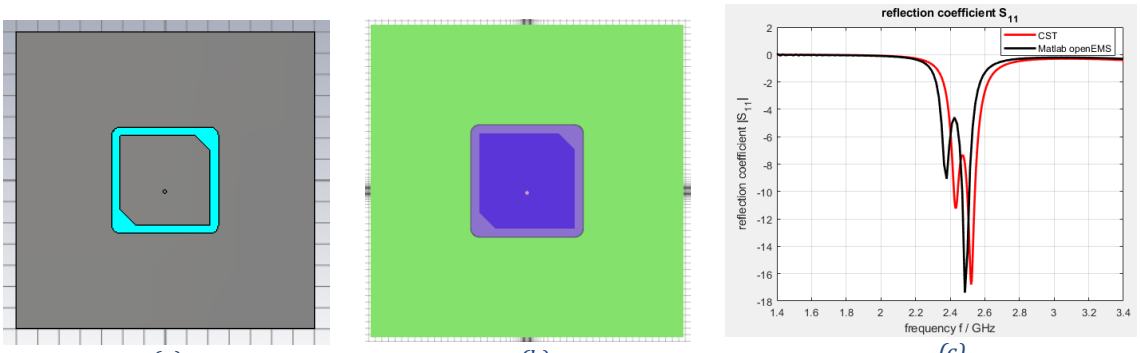

(a) *(b)* *(c)*

Figure 4.5: Step 3: a) CST studio suit design, b) MATLAB openEMS design, c) S11 parameter – comparison between both software.

Step 2 to 3 analysis: Adding bending at the substrate corners did not represent a substantive change from past design.

4- Same as (3), shifting the patch (Incorrect)

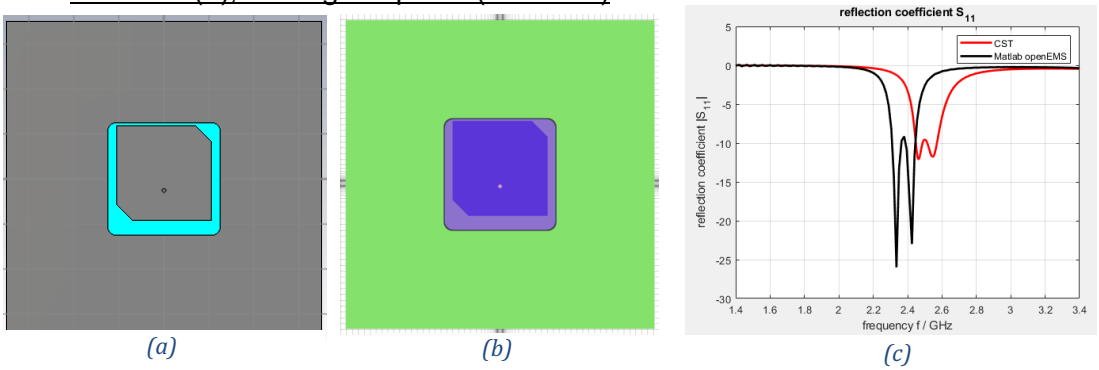

(a) *(b)* *(c)*

Figure 4.6: Step 4 (incorrect): a) CST studio suit design, b) MATLAB openEMS design, c) S11 parameter – comparison between both software.

After analysing the simulation results of the last change, we realised that the resonance peaks of MATLAB openEMS design were placed far away from the antenna specifications we were following. Therefore, it was necessary to analyze the code and suggest a suitable solution to overcome the frequency shift problem. The MATLAB file was checked and neither the excitation function nor the mesh was defined correctly. After correcting the code, the MATLAB openEMS antenna design performed at the correct frequency range as seen in green at the following Figure 4.7:

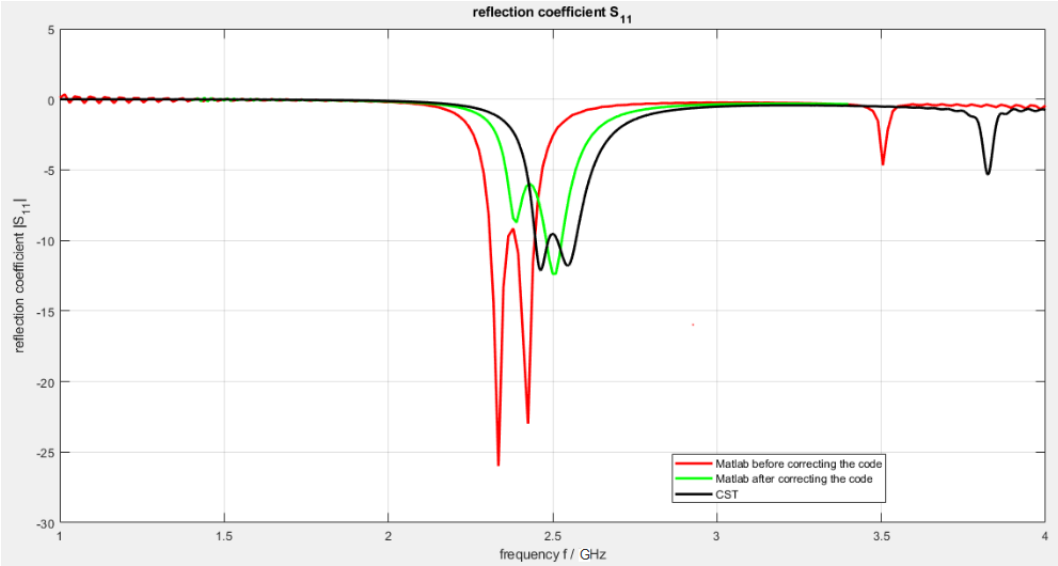

Figure 4.7: MATLAB openEMS code correction.

4- Same as (3), shifting the patch (CORRECTED)

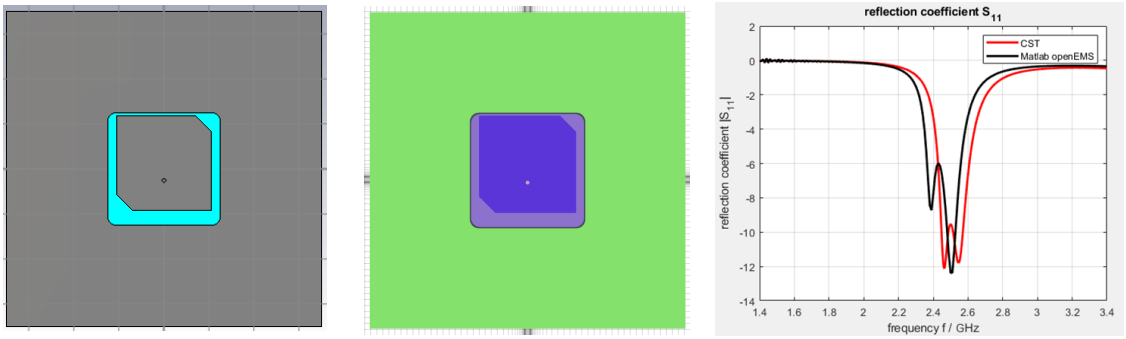

(a) *(b)* *(c)*

Figure 4.8: Step 4 (corrected): a) CST studio suit design, b) MATLAB openEMS design, c) S11 parameter – comparison between both software.

Step 3 to 4 analysis: Moving up the patch, the peaks started becoming similar in terms of amplitude. In step 3, there is much more depth difference between the two peaks compared with the step 4, where the peaks made almost equal. We achieved higher bandwidth for lower values of return loss. In short, the antenna is performing better.

5- Same as (4), with cylindrical ground plane

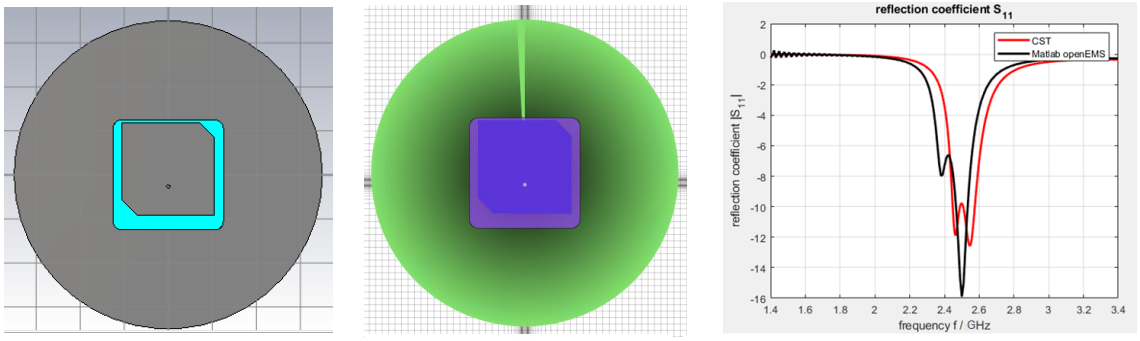

(a) *(b)* *(c)*

Figure 4.9: Step 5: a) CST studio suit design, b) MATLAB openEMS design, c) S11 parameter – comparison between both software.

Step 4 to 5 analysis: Changing the ground shape from square to cylindrical was not a big enhancement. The cylindrical ground plane contributed to improve a little bit the antenna design bandwidth due to the second peak is deeper. In fact, S11 shape with cylindrical ground plane is worse compared with the square ground plane design.

6- Same as (5), with aluminium ring around the patch

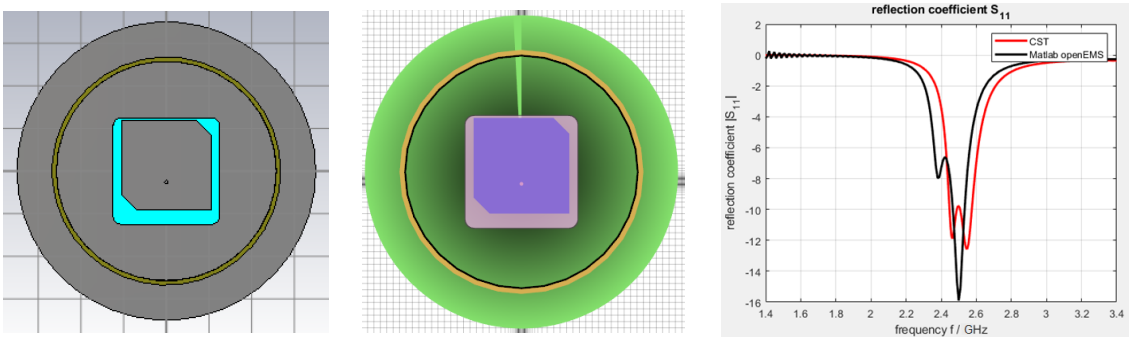

(a) *(b)* *(c)*

Figure 4.10: Step 6: a) CST studio suit design, b) MATLAB openEMS design, c) S11 parameter – comparison between both software.

Step 5 to 6 analysis: With adding a ring of diameter equal to 50 mm and width equal to 1mm, we wanted to verify if it would represent a big deterioration in S11 parameter. If it represents, the ring as an isolation enhancement will not be tested. Comparing Figure 4.9(c) and Figure 4.10(c), there were not big differences between the antenna design without the ring and the antenna design with the ring. Therefore, at that time, the option of adding rings as isolation structure was not rejected.

7- Same as (5), adding a ground box of Sandy Soil

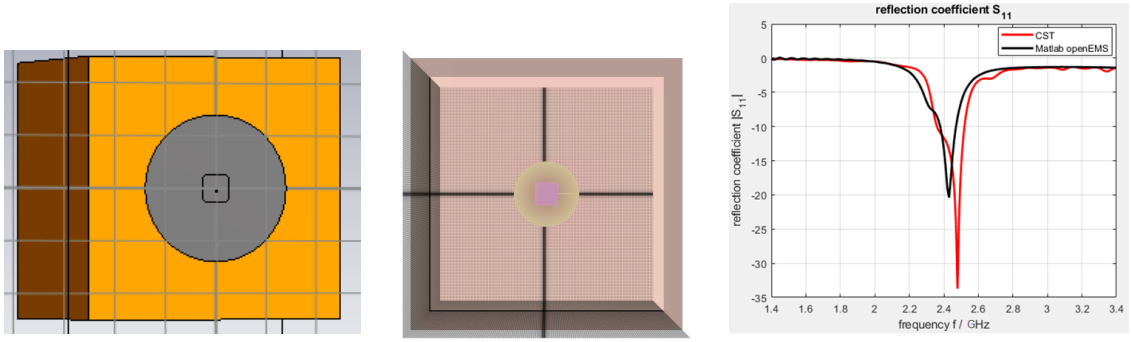

(a) (b) (c)

Figure 4.11: Step 7: a) CST studio suit design, b) MATLAB openEMS design, c) S11 parameter – comparison between both software.

Step 6 to 7 analysis: At this step, we wanted to test how the antenna works ahead of a ground box. There was a notable difference between the other figures. Instead of two peaks, only one peak appeared. Also, it can be seen at the Figure 4.11 (c), the resonance peak is placed at a lower frequency, this is due to the relative permittivity of the material is higher than the air relative permittivity. At the Eq. (4.1), lambda is a fixed value which depends mainly on the antenna dimensions, therefore, the higher the permittivity, the lower antenna operation frequency.

$$Frequency = \frac{v_p}{\lambda} = \frac{c_0}{\sqrt{\varepsilon_r} \cdot \lambda} \tag{4.1}$$

parameter v_p is the propagation speed in the medium.

8- Same as (5), adding a ground box of concrete

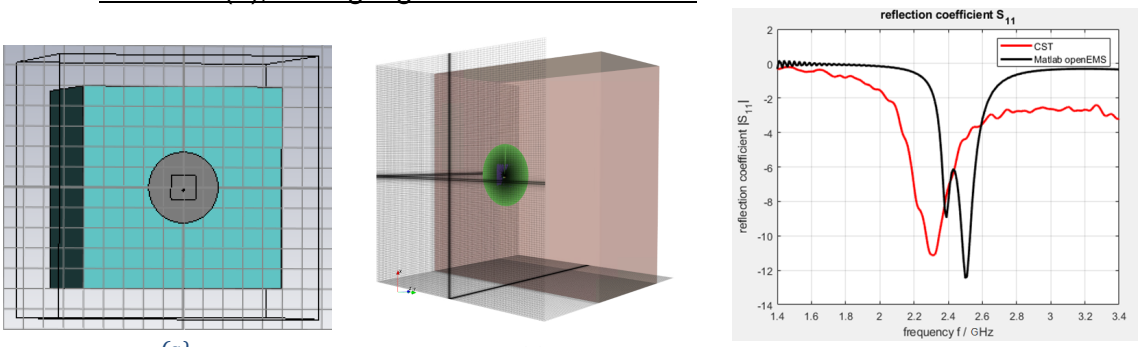

(a) (b) (c)

Figure 4.12: Step 8: a) CST studio suit design, b) MATLAB openEMS design, c) S11 parameter – comparison between both software.

Step 7-8: At last step, the material ground box was changed compared to the previous step 7. As shown in the Matlab openEMS black line of the Figure 4.12(c), there are two peaks instead of one like step 7. Depending on the material characteristics, the antenna will behave in different manner. Another important conclusion to draw from this last step, CST software did not work correctly with the concrete box added, after few tests repetitions, CST student license was not able to face simulations with big scenarios.

From all the modifications applied to the antenna design, the conclusion is that cutting the corners of the patch antenna was by far the most important enhancement because of the bandwidth growth. The verification of what section 3.3.1.1 reflects about bandwidth improvement read it in the papers is done with the software simulation results added. Moreover, moving up the patch also made a slight improvement in antenna bandwidth and return loss. Finally, it can also be draw from the results that the performance of the antenna depends directly on the ground material characteristics.

4.1.3. Software comparison conclusions

Even though we have used the same dimensions for both software designs, we can see at the different steps figures that there is a little frequency shift and also the peaks depths are different between CST and MATLAB designs. This might be due to the slightly different simulation techniques that both software use. Below is the analysis of the main differences between CST and MATLAB openEMS.

One of the biggest differences concerns the mesh generation. We could see for a little change in mesh size, no matter how small it may be, impacts the simulation results.

In the case of CST time domain solver methods, the software automatically creates a hexahedral mesh. Also, CST software generates automatically the different mesh lines distances depending on the different design needs. On the other hand, in MATLAB openEMS, the whole mesh is manually defined. We should generate all the mesh lines axis by axis as well as determine the mesh resolution values.

Similar issue happens with the simulation box. In CST design software you need only to set the kind of boundary conditions you want and then all the details pertaining the simulation domain size will be taken care of by CST. While in MATLAB openEMS you define the simulation box dimension manually.

Even if we have seen that there are some obvious differences between both software and therefore the simulations results are not exactly the same. We can safely say that the results should be regarded as a satisfactory work considering that in both software, the simulation result are very close to each other as well as close to how the antenna prototype datasheet shows.

At this point, our initial question can be answered, MATLAB openEMS has proven to be successful software for antenna designing and it can also be compared with the simulations results obtained with the recognized HF-simulation software CST Studio Suite.

Furthermore, we found out that when we added the ground box at the antenna design, the software CST had a lot of dimensions constrains because we were using a student license. Consequently, it was not possible to do the ground box as big as we want with CST because the software was not able to prepare the simulation scenario for such dimensions. Conversely, we could do simulations with ground box as big as we want with MATLAB openEMS. For that reason, when we need to do simulations with a ground box, we would rather use MATLAB openEMS instead of CST.

4.2. Final antenna design

After all the analysis, we decided to keep working with the square patch antenna with square ground plane because it was the design that performed best at the frequency interval of interest (between 2.4 and 2.5 Hz) and it was also the most similar in terms of simulation results to the antenna prototype datasheet (figure 3.3). The dimensions of the antenna components are the same specified in Table 4.1.

In order to have more precise information about the final antenna design, the following shows several angles and the most important behaviour charts of the antenna design as well as some coaxial connector angles. These figures were taken from MATLAB openEMS.

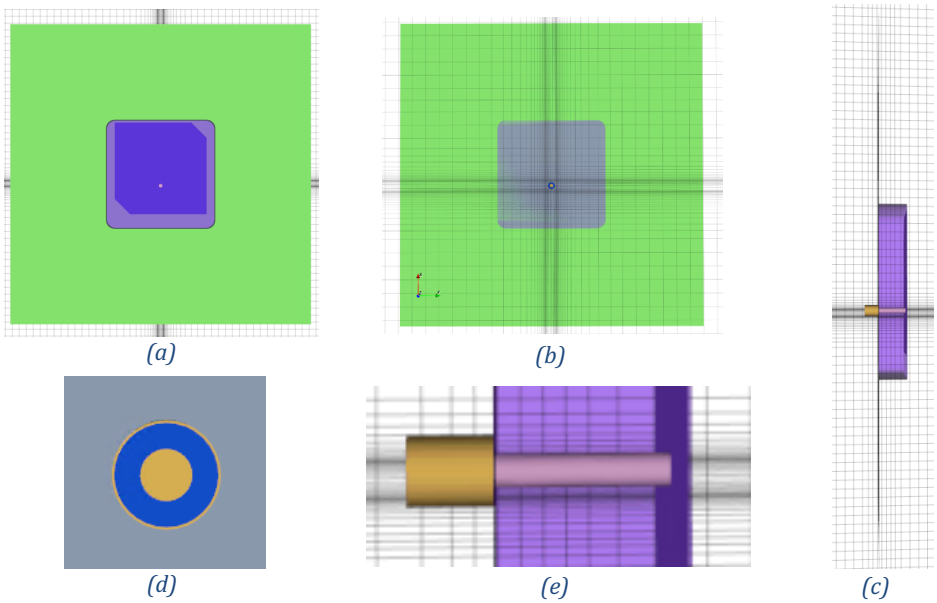

Figure 4.13: MATLAB openEMS final design: a) front view of antenna design, b) back view of antenna design, c) profile view of antenna design, d) front view of coaxial connector, e) profile view of coaxial connector.

The simulation results were also carried out using MATLAB openEMS:

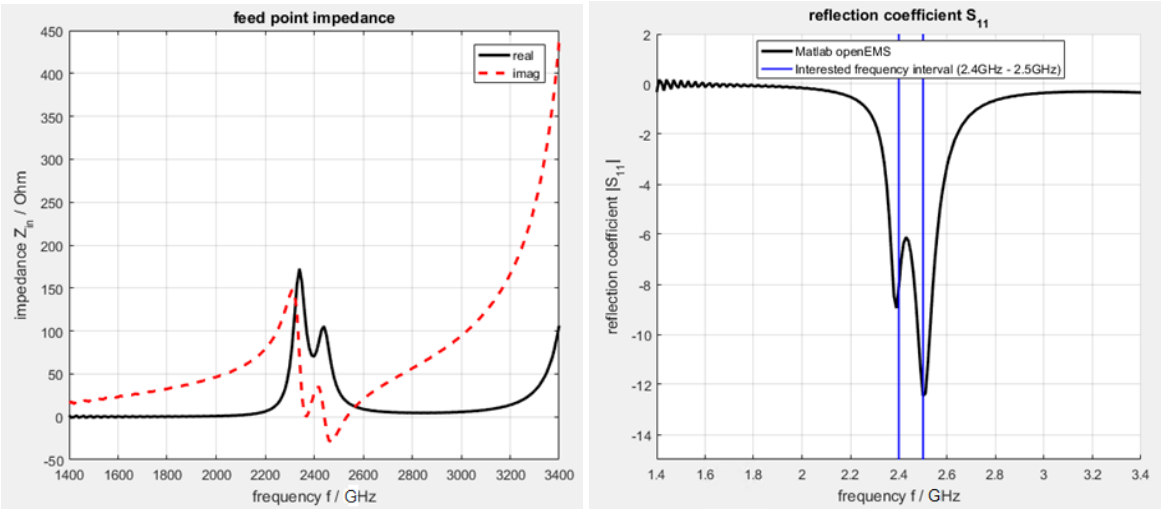

(a) (b)

Figure 4.14: Final antenna design: a) feed point impedance, b) S11 parameter - the interested frequency interval is delimited in blue vertical lines (2.4-2.5GHz).

The real part of the impedance should be 50 Ohm and Figure 4.14 shows 175 Ohms for 2.4 GHz and 100 Ohms for 2.5GHz. In the case of imaginary part, the aim was to get 0 Ohms and we were almost there, although there is still room for improvement. Therefore, an impedance transformation network might be needed in order to have perfectly matched antenna. Regarding the Figure 4.15, the resonance frequencies are at the correct place because they are at 2.39GHz and 2.5GHz and the resonance peaks of the antenna prototype datasheet are almost to 2.4GHz and 2.5GHz as well.

The simulated 3D radiation patterns at the two resonance frequencies (2.39GHz and 2.5GHz) of the MATLAB openEMS antenna design are shown in the following figures:

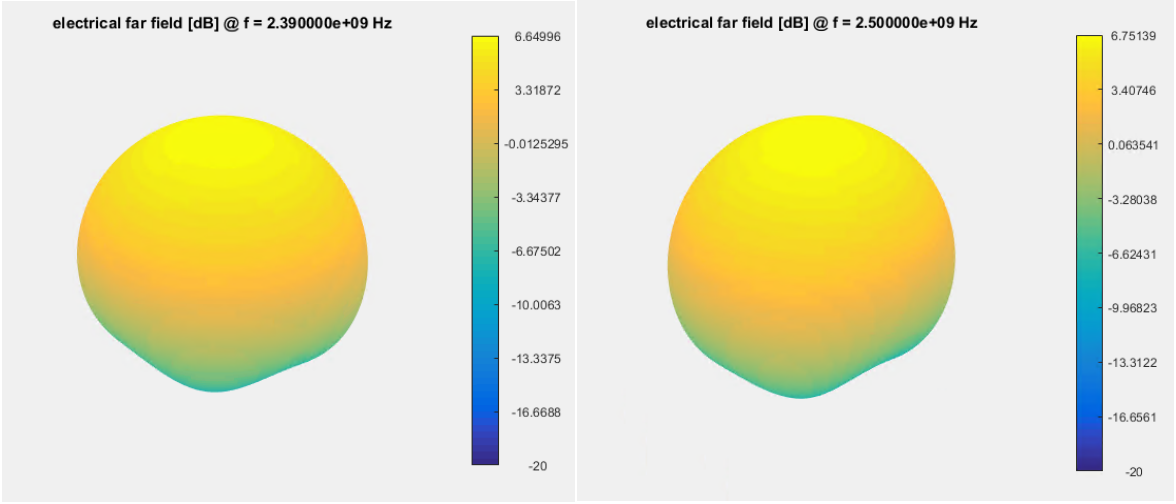

(a) *(b)*

Figure 4.15: 3D radiation pattern of the final antenna design: a) at first resonance peak (f=2.39GHz), b) at second resonance peak (f=2.5GHz).

A comparison between MATLAB openEMS and CST software of 2D radiation pattern at the resonance frequencies is shown with the figures below:

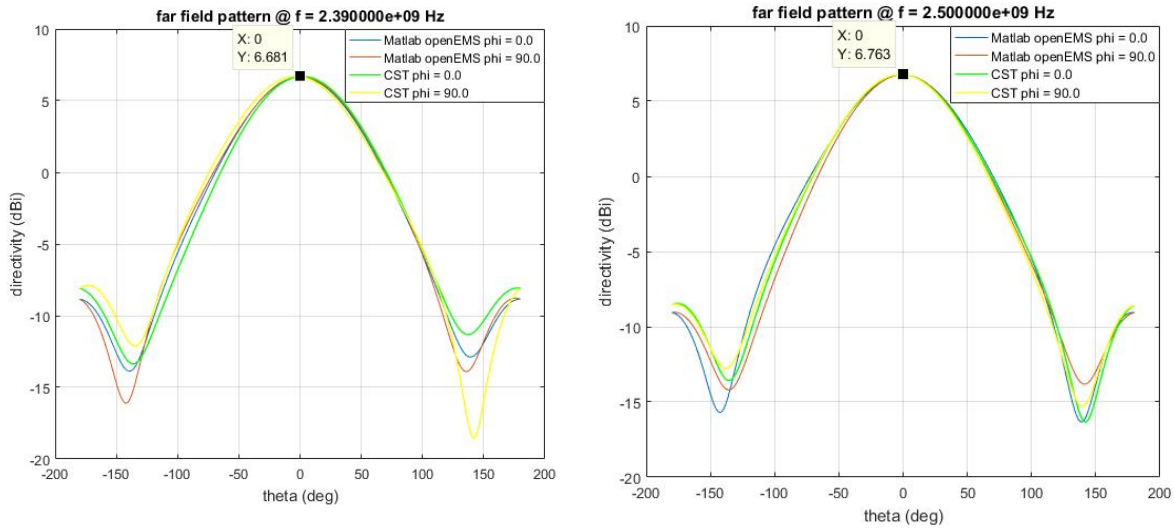

(a) *(b)*

Figure 4.16: 2D far field pattern – comparison between MATLAB openEMS and CST: a) first resonance peak (f=2.39GHz), b) second resonance peak (f=2.5GHz).

As it can be seen in Figure 4.16, the radiation patterns are almost equal in MATLAB openEMS and CST. Despite the differences between the two software already mentioned, both antennas designs have the same radiation pattern.

Compared with the antenna prototype datasheets, the results above show that they are a little worse in terms of gain. The maximum directivity achieved from software simulations is 6.8 dB and considering an 80% of efficiency as datasheet specified:

$$Antenna\ Gain = Directivity * Antenna\ efficiency = 6.8 * 0.8 = \mathbf{5.4\ dB} \quad (4.2)$$

The antenna design gain is 5.4 dB; therefore, software antenna designs are 1.1 dB lower than the 6.5 dB of the datasheet antenna prototype gain specification.

The MATLAB openEMS code of the final GPR antenna design is in section 8.1.

4.2.1. Definitive antenna design comparison between software and hardware

After completing the software antenna design analysis, some experimental analysis were conducted. We manufactured the final antenna design mentioned at the previous section in order to verify if the performance of antenna in real experiments are similar to the performance of the antenna simulations. We had two antennas of the prototype, so we examined individually both in two different scenarios:

(a)

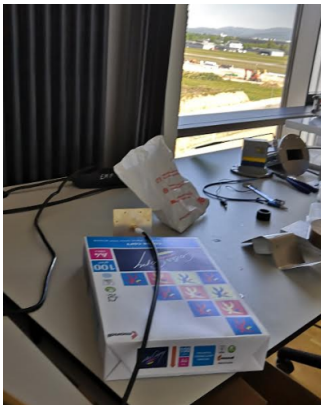

(b)

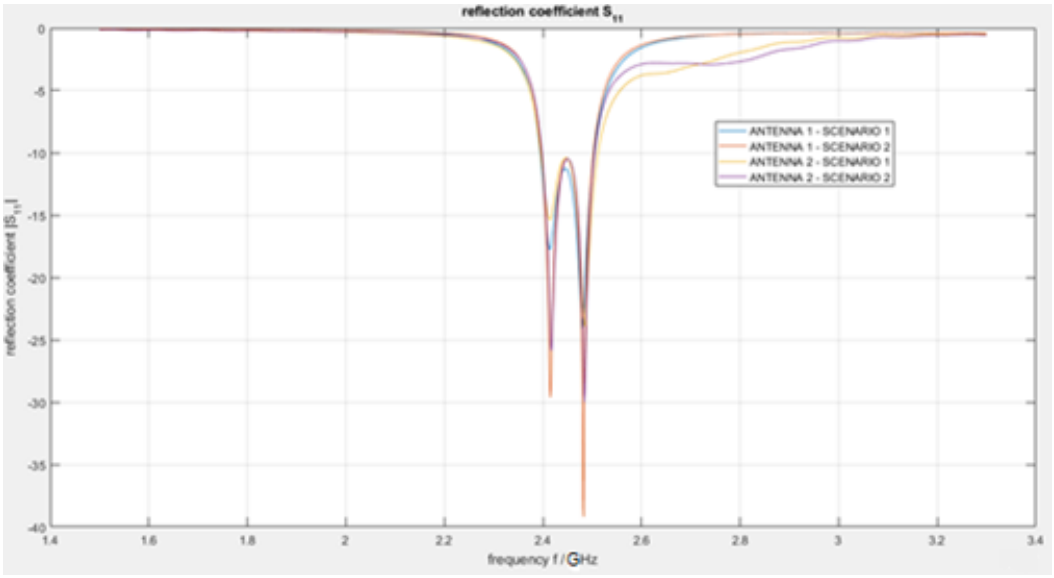

(c)

Figure 4.17 Experimental results of the antenna designed: a) scenario 1, b) scenario 2, c) S11 parameter of the two antennas in two different scenarios.

Comparing the experimental results with the simulation results, it was confirmed that both results have similar S-Parameter shape and almost the same resonance frequencies. Therefore, we can be certain that the GPR antenna design simulation using the antenna design were correct. However, there is a big difference between experimental and simulation results in terms of return loss; the manufactured antenna has return loss values near to 40dB while with the software design while we got maximum values of 13 dB. This large difference is due to our software antenna designs are reflecting too much power because it is not very well matched. We still have to add an impedance transformation network which could give a big enhancement in return loss values.

We also did some simulations with the antenna touching two different ground materials: brick and ceramic plate. As the last simulations, we had two antenna prototypes, so we examined individually both in two different orientations for each material:

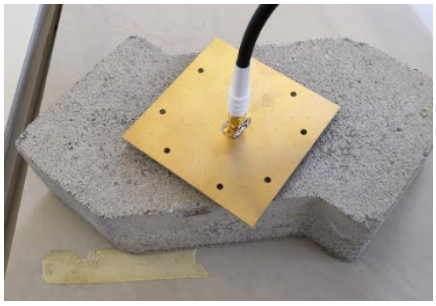

(a)

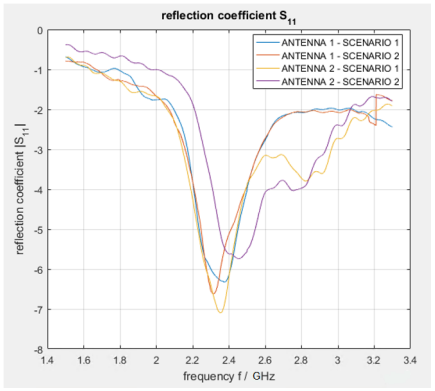

(b)

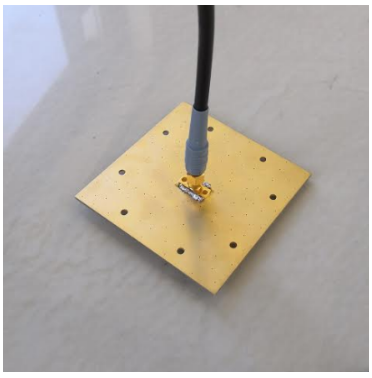

(c)

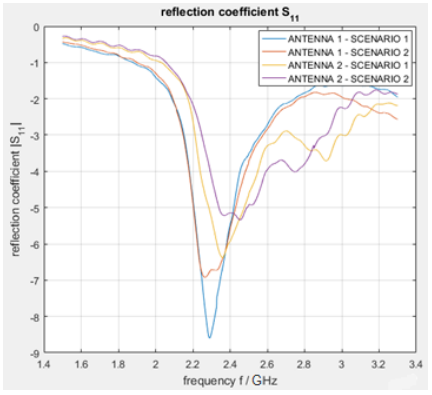

(d)

Figure 4.18: Antenna manufactured experimental results: a) set up – antenna pointing on a brick, b) S11 parameter of the two antennas in two different scenarios, c) set up – antenna pointing on a ceramic plate, d) S11 parameter of the two antenna in two different scenarios.

If we compare figures above with the results obtained in section 4.1.2 (steps 8 and 9) when we added two different ground boxes at the software antenna design, the performance of the antenna is very similar. The antenna peaks in both cases started getting closer to each other and the return loss values are lower. In addition, the resonance frequency is placed in lower frequency, this fact is due to the relative permittivity of the material is higher than the air relative permittivity. As we can see in Formula 4.1, as lambda is fixed value which depends on the antenna dimensions, the higher the permittivity, the lower antenna operation frequency.

Finally, as can be seen in both figures above, the performance of the second antenna at the second scenario (purple line) is a little worse that the others, this may be because when the experimental simulations were done, we didn't put as correct the antenna as the other cases and there was a little air gap between the antenna and the material tested.

4.3. GPR antenna assembly analysis

In this section, different GPR antenna designs are analyzed by means of CST Studio Suit software. Two exactly antenna equal to the previous section were used for designing the radar (Square ground plane of 70x70 mm); one antenna works as transmitter and the other one as receiver.

The main objective in the section is to carry out different design modifications and add isolation structures in order to find which is the best GPR antenna design for our project.

4.3.1. CST Parameter sweeps of GPR antenna modifications

The aim in this part is to deduce which are the best GPR antenna assembly design characteristics and dimensions. From find out about the distance between the antenna Tx and the antenna Rx to knowing the best groun plane dimension.

4.3.1.1. Two ground planes: changing the distance between both antennas

First of all, we wanted to analyze how the distance between the two GPR antennas influence the S-parameters. A parameter sweep changing the distance between the centre of the Tx-antenna and the Rx-antenna was done, from 70 mm (touching each other sides) to 200 mm, with a step width of 10 mm.

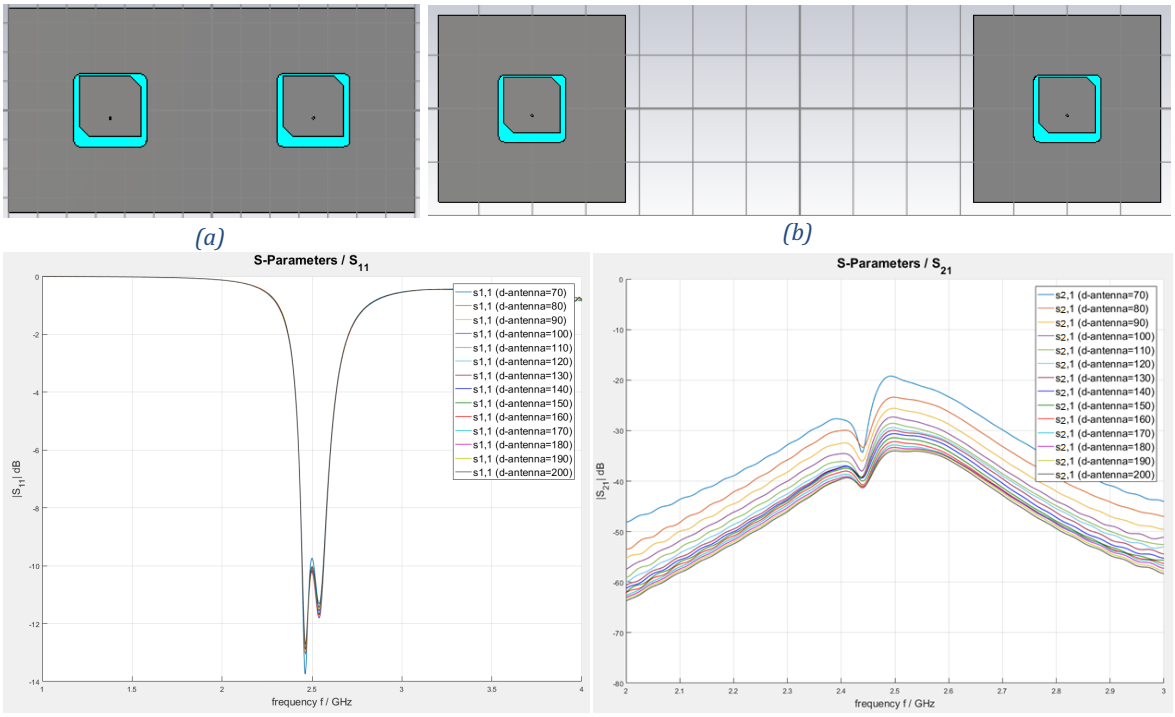

Figure 4.19: GPR antenna design with two ground planes: a) distance between both antenna= 70mm, b) distance between both antenna= 120mm, c) S11 parameter of the different distances, d) S21 parameter of the different distances.

In Figure 4.19 (c), it can be seen that there is not much different between S11 parameter at the different distances. No matter how long the distance between the antenna is, the antenna will be the same and it will perform almost equal always.

For analyzing the isolation between the radar antenna, we will be focus on S21 parameter. In Figure 4.19 (d), as the distance between antennas increases, the S21 parameter decreases. It is reasonable that when the distance increases, the isolation between the antenna is better (lower values of S21). But the most important issue is to decide which distance will better fit our design. It must be taken into account that the bigger the distance, the more difficulties to add the GPR antenna assembly at the drone.

Comparison between CST design and experimental results

Next, the same distances parameter sweep did in the previous section was done at the IMTEK Laboratory with the exactly GPR antenna dimensions of the software design. In this section, only the S21 parameter is analyzed cause is the one that experienced more changes while modifying the distance. Also, for evaluating the isolation enhancement, it is the most important parameter:

(a)

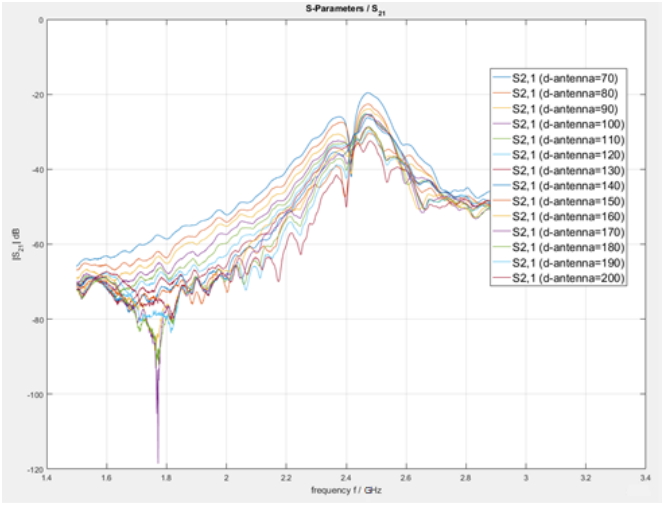

(b)

Figure 4.20: GPR antenna manufactured: a) set up, b) S21 Parameter of the different distances.

Comparing the experimental results with the CST simulation results, it is seen both behaves very similar. There are no significant differences in S21 values and shape for the different distances. However, it is important to evaluate how is changing the parameter S21 while increasing the distance between antenna centers in order to find an optimal value for the GPR antennas distance. Therefore, a deeper analysis of the S21 values according to the different distances used in the simulations was done.

Analysis of |S21| according to distance between both antennas

The behavior of the maximum values of S21 parameter with respect to the distance between Tx and Rx antenna is plotted in order to find the distance which fits best for the GPR antenna. In Figure 4.21, the changing over distance is not linear. Therefore, the optimal distance between antennas is when the slope is inclining because it represents better isolation while the distance increases, but increasing the distance can also cause an overweight problem. Therefore, strike a balance between distance and weight is needed.

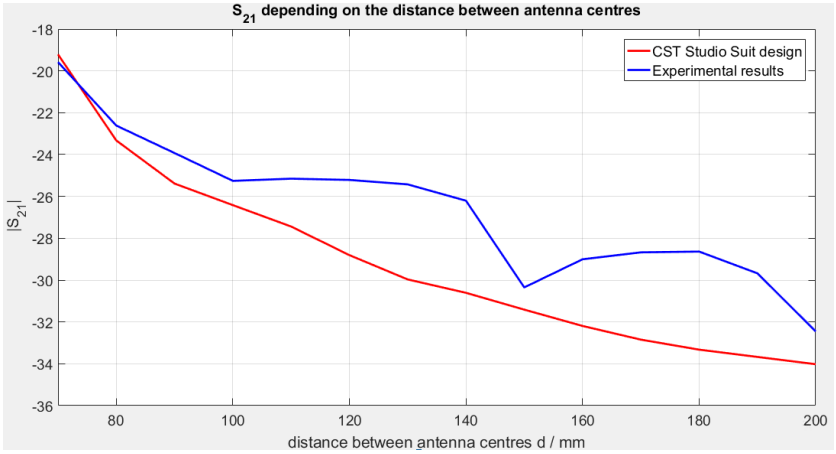

Figure 4.21: Comparison between CST design and experimental results of |S21| according to distance between antenna of GPR antenna with two ground planes.

As shown in Figure 4.21, the shorter is the distance, the more drastically S21 parameter change. Above 100 mm, the S21 function slope starts getting flat. Therefore, the distance between antennas from 80 to 100 mm seems to be a good option for the design. Besides, this range of distance is not too big for introducing the GPR antenna on the drone.

4.3.1.2. Two ground planes: changing the ground planes size

The second analyzed parameter was the ground plane dimensions, as we have already said, the two-ground plane are squares. We modified the sides from 70mm to 100mm, with a step width of 10mm in order to find out which dimension fit best for the design.

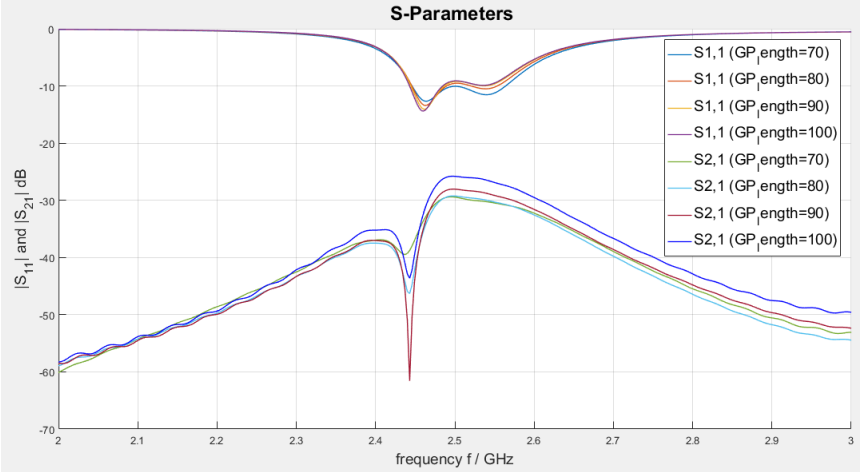

Figure 4.22: S-parameters of the different ground plan dimensions.

The values above 80mm were dismissed because they achieved worse isolation results. As it can be seen, in the case of ground plane with sides equal to 80mm, the results are slightly better, so we kept this size value for the ground planes.

4.3.1.3. Sole ground plane: changing the distance between both antennas

Analysis of |S21| according to distance between both antennas

For the good performance of the mobile GPR node, it will be better to have both antennas on the same ground plane structure. By doing so, it is ensured that both antennas will point to the same direction and the distance between them will be always the same.

In this section the behavior of the GPR antenna in only one ground plane of width = 80mm and length= distance between antenna centers (d) + 80mm was analyzed. The same analysis of the 4.3.1.1. was done. We examined how the S21 parameter is developing while the distance is getting longer. The distances were from 70 mm to 200 mm, with a step width of 10 mm. Moreover, the plot of the S21 parameter according to the distance between the two antenna is shown in 4.23 (c).

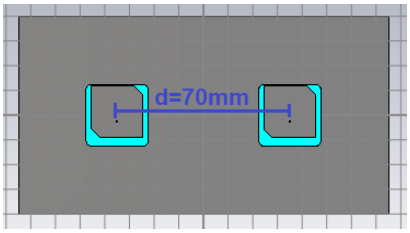

(a)

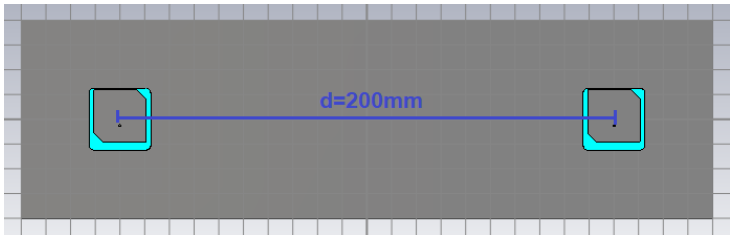

(b)

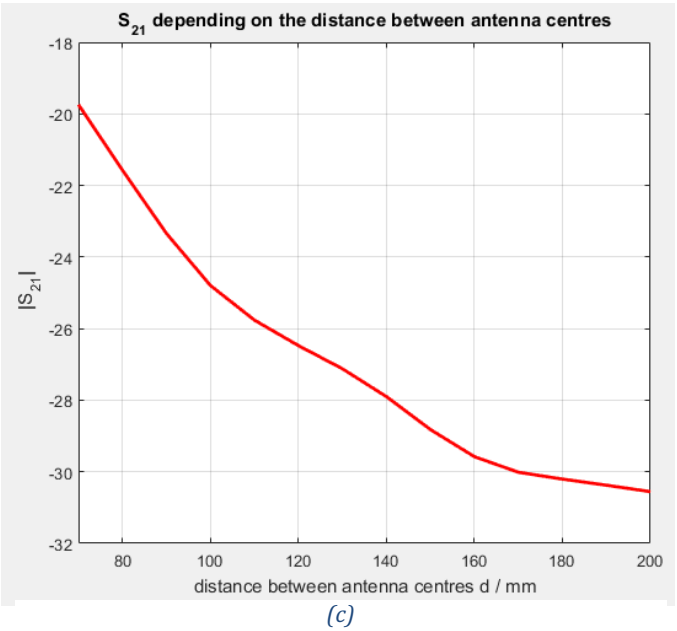

(c)

Figure 4.23: GPR antenna design with one ground planes: a) distance between both antenna= 70mm, b) distance between both antenna= 120mm, c) |S21| according to distance between antenna of GPR antenna with only one ground plane.

There is no big difference between the two-ground plane simulation analyzed in section 4.3.1.1. Similar conclusions are drawn from the figures.

Figure 4.23 (c) shows that when the distance increases, the isolation is improving and the shorter is the distance, the more drastically S21 parameter change. Similar optimal values of GPR antennas distances were obtained compared with the previous section, but in this case, the optimal distance range is bigger. At the distance equal to 120 mm, the desing still have inclining slope. Therefore, the optimal distance between antennas range in this section is from 80 to 120mm.

But the matter now is that we should also take into account the design weight. As the distance increases, the GPR antenna assembly is heavier. For that reason, our main goal was then to find a good technique for isolation enhancement in short distances and therefore trying to reduce the design weight.

4.3.2. CST parameter sweeps with different isolation structures

The following shows the result of difference implementation of structures for isolation enhancement. The objective of this section is to find out an isolation structure which will allow us to reduce the distance between the two GPR antenna and thus also reduce the antenna assembly weight while having good isolation improvement.

The parameter sweeps analysis of the following sections were carried out using CST Studio Suite, nevertheless, the section 8.1 shows some MATLAB openEMS codes of the GPR antenna with isolation structures.

4.3.2.1. Analysis of CST design adding rings

To verify the rings effect on isolation enhancement in our GPR antenna, we searched some electronic components suppliers. We found an interesting aluminum rings which fitted perfectly for our design dimensions. The rings dimensions were, outer diameter (mm) x thickness (mm): 40x2, 50x2 and 60x2. The different CST design with 40x2, 50x2, 60x2 mm rings at antenna distance of 70mm is shown in Figure 4.24 (a), (b) and (c).

The behavior of the GPR antenna was analyzed with the three different rings. We proceed doing a parameter sweep of the distance between the antenna from 70 mm to 200 mm, with a step width of 10 mm. Later, a plot of the different maximum |S21| values of the designs with rings according to the antenna distance was done and finally, the results were compared with the design without rings as shown in Figure 4.24 (d).

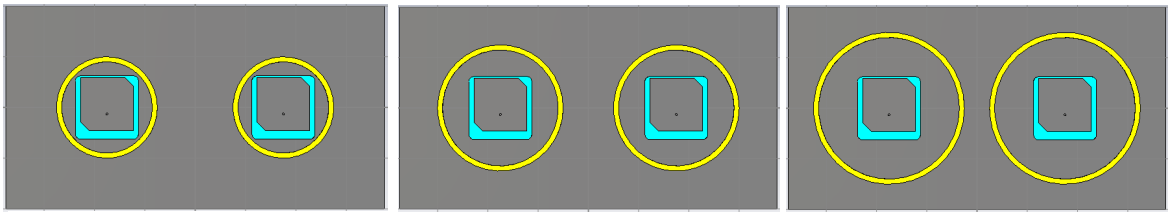

(a) *(b)* *(c)*

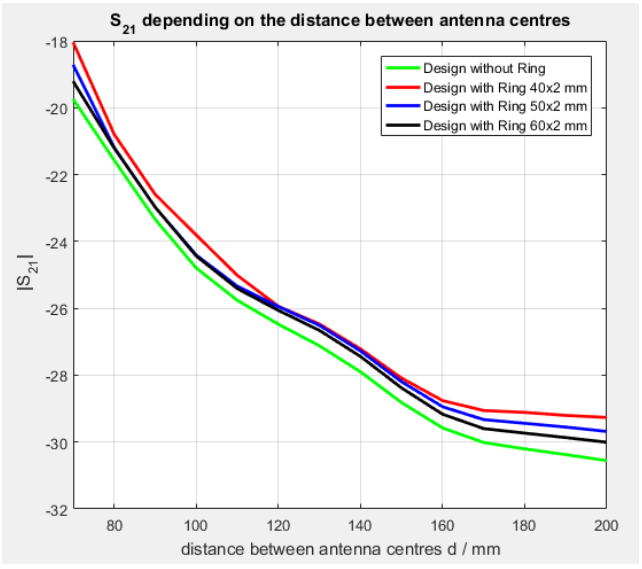

(d)

Figure 4.24: GPR antenna design adding rings at the distance between both antenna= 70mm: a) 40x2 mm, b) 50x2 mm, c) 60x2mm, d) analysis of |S21| according to distance between antenna of GPR antenna with one ground plane and with rings.

In the Figure 4.24 (d) above, the green line is the one that is having lower |S21| values, and therefore, better isolations. As the green line corresponds to the design without ring, the design with rings did not mean an isolation enhancement, hence the option to add rings in our GPR antenna for improve the isolation was dismissed.

4.3.2.2. Analysis of CST design adding meander-line structure

An slotted meander-line for isolation enhancement was found. The problem was that there is not any specification of how compute the different parameters associated at this structure. In paper [17] they worked with the frequency of 4.8Ghz which is twice the frequency we used (2.4GHz). Therefore, the meander-line was designed with exactly double the dimensions that the paper used. The meander-line is composed of 2 different components: meander-line PEC piece and FR4 box of 50x6x4mm for supporting the meander-line. The following Figure 4.25 shows a top view of the GPR antenna design adding the meander-line isolation tecnique:

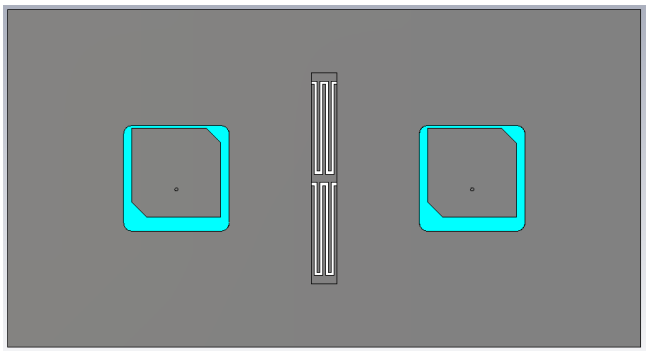

Figure 4.25: GPR antenna design adding slotted meander-line structure.

In this case, the maximum S21 parameter values according to the distance between antennas were not compared because the S21 function has a lot of drastic changes. Therefore, the maximum values of S21 parameter can be placed at frequencies very different and out of the interested frequency range. At the following section 4.3.2.4. all the isolations structures S-Parameters are analyzed.

4.3.2.3. Analysis of CST design adding EBG structure

Using the formulas from the papers [18] and [19] and at the frequency of 2.4GHz, the EBG isolation structure has the following dimensions: EBG square structure has been tried for the side values of 9,12,15,18; four cylinders with radius=0.625mm that connect the EBG square structure with the ground plane, FR4 box with 4 holes for the cylinders and the gap between EGB structures is equal to 0.5mm. The following Figure 4.26 shows a top view of the GPR antenna design adding the different dimensions of the EBG structure used:

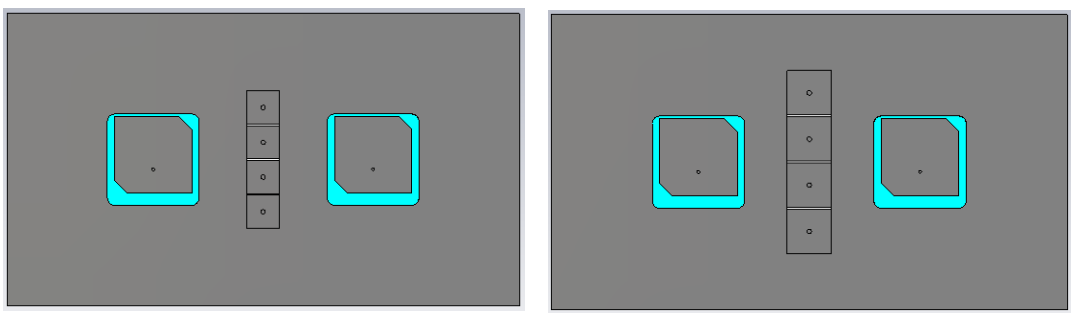

(a) *(b)*

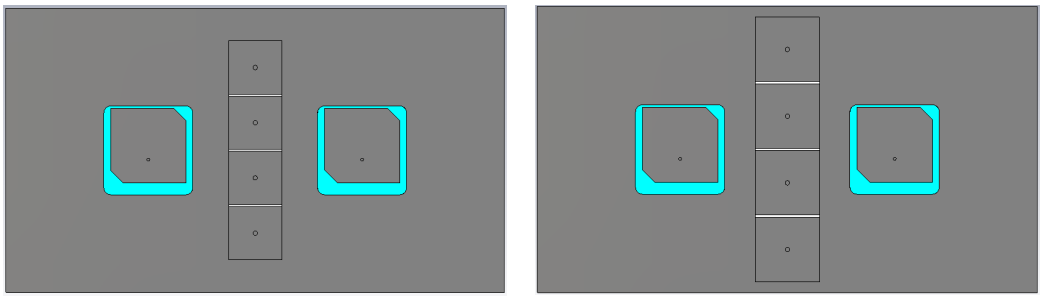

(c) (d)

Figure 4.26: GPR antenna design adding EBG structure with different square side: a) 9mm, b) 12mm, c) 15mm, d) 18mm.

In this case we also decided not to compare the maximum S21 parameter values with respect to the distance between antennas, because S21 functions has a lot of drastic changes. It does not make sense to compare the maximum values obtained for each distance because the it can be placed in completely different frequencies. At the following section 4.3.2.4. the EBG isolation structure S-Parameters are analyzed.

4.3.2.4. Comparison with all the isolation techniques applied

The following shows the S-parameters of all the techniques applied at the GPR antenna for isolation enhancement. Two distances very different from each other were analyzed in order to see the performance of the designs in two completely different scenarios. The distances between antenna centers selected were equal to 70 and 110 mm. The blue vertical lines are placed at the resonance frequencies, they mark out the area of interest.

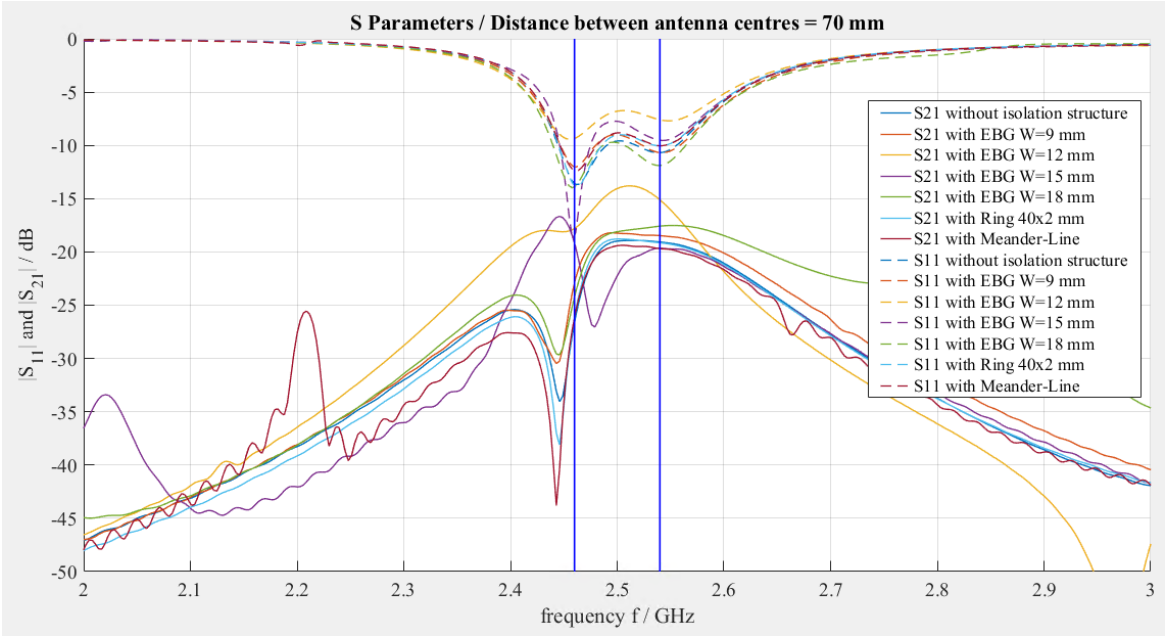

(a)

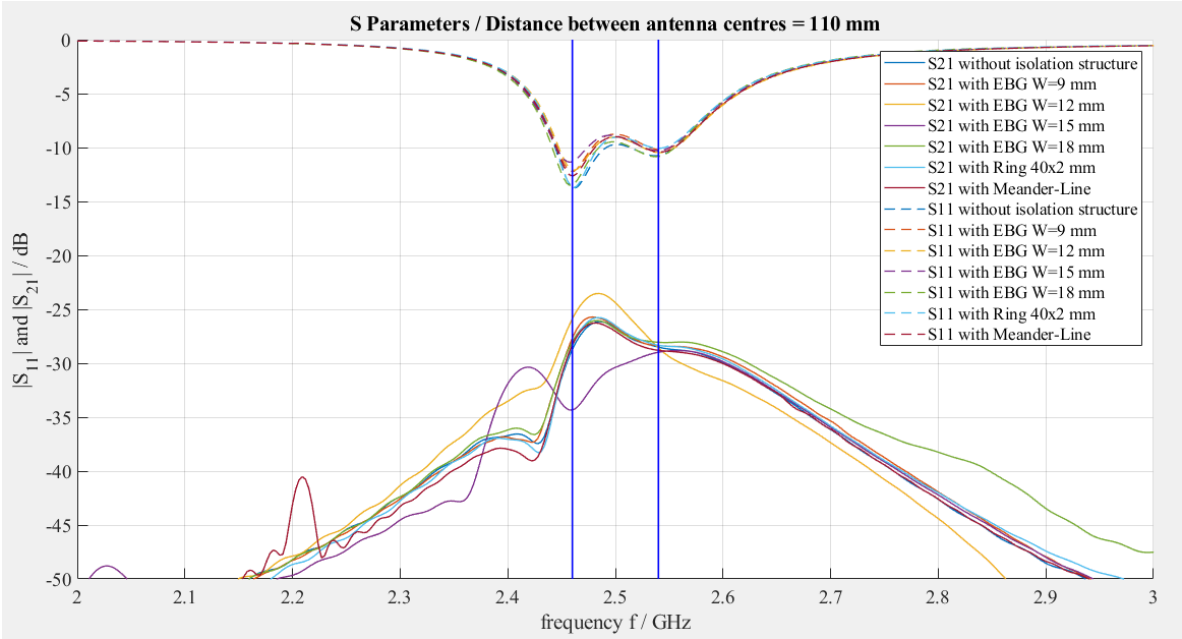

(b)

Figure 4.27: S parameters of all the isolation techniques: a) distance between both antennas=70mm, b) distance between both antennas=110mm.

Analysing the simulation results between the two resonance frequencies in Figure 4.27 (a) and 4.27 (b), the following conclusion was made:

	S11 Parameter	**S21 Parameter**
Distance = 70 mm	-Almost all the designs have the same S11 shape -The first peak of the EBG=15mm design is the deepest	-The meander line design is quite better than the rest, except of the design with EBG=15mm -The EBG=15mm design has way more isolation than the rest
Distance = 110 mm	- All the designs have the same S11 shape	- The EBG=15mm design has the best isolation by far than the rest designs

Table 4.2: Results analysis of all the isolation techniques applied at the GPR antena.

The EBG with square sides of 15 mm (purple line), for the two distances evaluated achieved very good isolation enhancement compared with the rest techniques.

However, only at the distance equal to 70mm, the S11 parameter of the EBG with square sides of 15 mm has a slight worsening in terms of bandwidth. Even though this fact, this design is evaluated as the best option for the GPR antenna due to its surprising notable improvement in isolation (low values of S21 parameter).

After seeing the good results from the EBG=15mm, further details about this isolation structure were found out. We wanted to verify whether the isolation enhancement also happens in more distances. Therefore, a parameter sweep changing the distance between the centre of the Tx-antenna and the Rx-antenna with the EBG=15mm was done. From 40 to 120 mm, with a step width of 20mm.

The following Figure 4.28 shows the S21 parameter comparison between the GPR antenna design with and without the EBG=15mm structure:

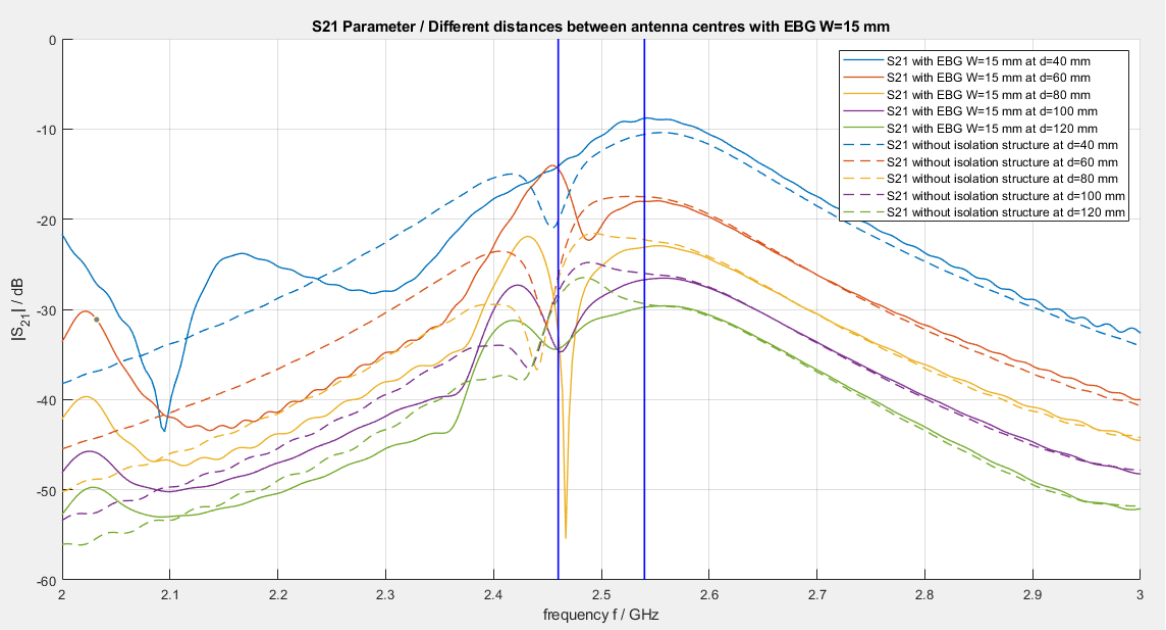

Figure 4.28: Comparison between the GPR antenna design with and without the EBG=15mm structure: S21 parameter.

A part from the distance between the two antennas equal to 40mm, which was the only where the performance of the design with EBG structure was worse than the design without isolation structure, the implementation of the EBG with square sides of 15 mm was improving the GPR antenna design isolation. Therefore, the design with the EBG structure in different distances was manufactured in order to know if the design can obtain the same isolation enhancement in realistic experiment.

4.4. Final design analysis

Summarizing all the GPR antenna analysis, we have seen in section 4.3.1.3 that the GPR antenna with one ground plane had good isolation at the distances between both antennas from 80 to 120mm. But later, it was found out that EBG=15mm had better results than the rest isolations techniques and also better results than the design without isolation technique with one ground plane in almost every distance. Therefore, we decided to manufacture the GPR antenna design adding the EBG isolation structure. Besides, the design with EBG=15mm also had very good isolation enhancement when the antennas are very close to each other, so this implies that the GPR antenna assembly would be smaller and light, then, easier to put it inside the drone.

4.4.1. Definitive GPR antenna design

The definitive GPR antenna assembly of this thesis will be made adding an EBG structure for isolation enhancement between Tx-antenna and the Rx-antenna. The EBG structure has the following dimension: four EBG square with the side values of 15; four cylinders with radius=0.625mm; FR4 box with 4 holes for the cylinders; the gap between EGB square structures is equal to 0.5mm.

The EBG structure abovementioned will be tested in IMTEK Laboratory at the distances between antenna centers of 60, 80 and 100mm. The following Figure 4.29 (a) and (b) are a trimetric view of the EBG design with and without hiding the FR4 box. The distance between both antennas centers in Figure 4.29 is 60 mm:

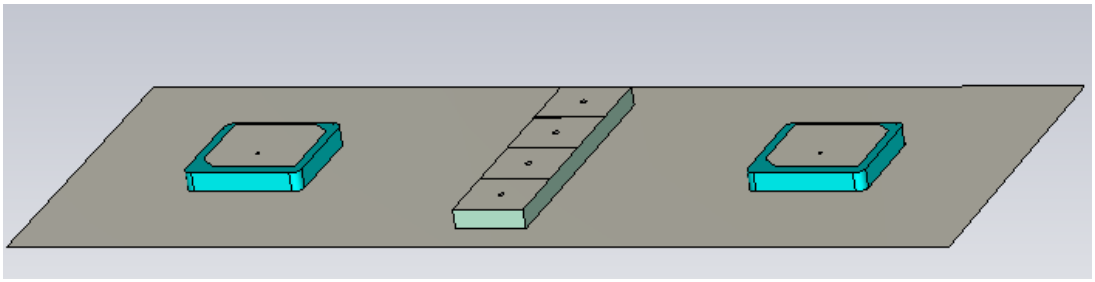

(a)

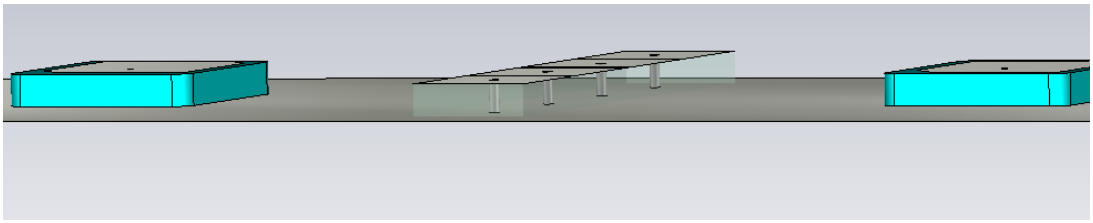

(b)

Figure 4.29: GPR antenna design with EBG=15mm: a) trimetric view, b) zoom in of profile view hiding the FR4 structure.

4.4.2. Comparison between CST design and experimental results

A comparison with manufactured GPR antenna and GPR antenna software design still has to be done. The aim of this section is to verify if the EBG=15mm can be as good in real life experiments as it has been in the software design, doing some experimental tests.

The comparison was not possible to do it before the limit date for delivery this report because the IMTEK laboratory have had some problem with the material online order and they are still not arrived. The intention is to work on it for adding the test results at the thesis presentation.

If the experimental results show good isolation enhancement, IMTEK department will carry out more specific experimental tests with the final manufactured prototype such us ground penetrating transmission test and ground penetrations transmission test for a setup with breathing robot. They will consider to use the prototype designed in this thesis for their project if the results in all the test are satisfactory.

5. Budget

The budget for this project is the following one:

	Wage/hour	Hours	Price per unit (Units)	Cost
Junior engineer	8 €/h	30 h/week	-	3.840 €
Senior engineer	20 €/h	5 h/week	-	1.600 €
Laboratory technician	16 €/h	20 h/total	-	320 €
Coaxial connectors	-	-	5.47 € (4)	21.88 €
RG174 cable	-	-	9.24 € (4)	36.96 €
Antenna prototype	-	-	3.27 € (4)	13.08 €
EBG structure	-	-	4.55 € (3)	13.65 €
TOTAL				5.845,57 €

Table 5.1: Project budget.

Firstly, the hours dedicated by the student (Junior engineer) and the tutor (Senior engineer) during the 4 months of the thesis project. Moreover, the hours that the IMTEK laboratory technician spent manufacturing the different designs tested.

Besides, the cost of the materials bought for the project are also included. The material specified above was for manufacturing the two antennas in different ground planes (First test did – Section 4.3.1.1.1) and the final GPR antenna design at three different distances (Second test remains to be done – Section 4.4.2).

In addition, I have used the software CST Studio Suit and MATLAB openEMS which a license should be paid in both cases, but as I worked with a student license and University license, I did not include them in the budget.

6. Conclusions and future development

The main goal of this project was to design a mobile GPR antenna assembly to detect trapped alive victims. We proceeded by analysing many design modifications and adding some isolation structures, in order to reduce the GPR antenna design crosstalk with the minimum distance possible between the Tx-antenna and the Rx-antenna.

Before finishing the design of the mobile GPR antenna, which is the main objective of this project, we have followed the path previously defined and consolidated the majority of objectives specified at the beginning of the project.

First of all, we learned how our antenna works due to a deep evaluation of each and every one of its characteristics which was made using two different software. In addition, it was possible to verify that apart from the CST Studio Suite software, which was already known to be widely used in other antenna designs projects, the Matlab openEMS software was very competent in antenna designing sector, obtaining practically identical results as the CST software.

Lots of analysis were carried out, modifying and incorporating structures to the GPR antenna. Whether the results turned out to be positive or negative was not the main concern, due to the fact that it has helped us to know our GPR antenna design better, and also to have the opportunity to compare with a lot of different GPR antenna designs. Moreover, these are investigations that IMTEK department has never done before and it will be very useful in future projects in this same field.

Sadly, not all the objectives set for this project were accomplished. Due to lack of time, some of the ideas that were discussed at the beginning were not implemented. For example, there was not enough time to design the impedance matching network and to do all the experimental tests proposed. However, knowing its importance, everything possible is going to be done before the final presentation, even if they are some basic experimental tests of the final GPR antenna and a design sketch of the matching network.

In conclusion, although the actual pandemic situation suddenly made us both change the place and the way of working, all the IMTEK members and I are very satisfied with the results obtained in this thesis. Although it was not possible to finish it, a very detailed investigation and a practically finished design was left. It may lead to a good antenna assembly ready to be used in real scenarios in case anybody from the same IMTEK department wants to continue with the investigation.

7. Bibliography

[1] D. J. Daniels, D. J. Gunton, and H. F. Scott, “Introduction to subsurface radar,” Proc. IEE, vol. 135, pt. F, no. 4, pp. 278-320, Aug. 1988.

[2] L. Peters, Jr. and J. D. Young, “Applications of subsurface transient radars,” in Time-Domain Measurements in Electromagnetics. New York: Van Nostrand Reinhold, 1986, ch. 9.

[3] L. Crocco and V. Ferrara, "A review on ground penetrating radar technology for the detection of buried or trapped victims," *2014 International Conference on Collaboration Technologies and Systems (CTS)*, Minneapolis, MN, 2014, pp. 535-540, doi: 10.1109/CTS.2014.6867620

[4] G. P. Radar, M. Robinson, C. Bristow, J. Mckinley, and A. Ruffell, “Suitability of GPR,” *Br. Soc. Geomorphol.*, vol. 5, pp. 1–26, 2013.

[5] E. C. Utsi, “Target Resolution Using Very High Frequency Ground Penetrating Radar,” *Struct. Faults Repair*, no. August, 2014.

[6] C. Balanis, “Advanced engineering electromagnetics,” 2012.

[7] J. H. Bradford, “Frequency-dependent attenuation analysis of ground-penetrating radar data,” *Geophysics*, vol. 72, no. 3, 2007, doi: 10.1190/1.2710183.

[8] K. Iizuka and A. P. Freundorfer, “Detection of Nonmetallic Buried Objects by a Step Frequency Radar,” *Proc. IEEE*, vol. 71, no. 2, pp. 276–279, 1983.

[9] A. Jimenez, “The Finite-Difference Time-Domain Method (FDTD),” *2-D Electromagn. Simul. Passiv. Microstrip Circuits*, no. 3, pp. 79–90, 2008, doi: 10.1201/9781420087062.ch4.

[10] S. D. Gedney, *Introduction to the Finite-Difference Time-Domain (FDTD)) method for electromagnetics*, vol. 27. 2011.

[11] J. H. Bradford, “Frequency-dependent attenuation analysis of ground-penetrating radar data,” *Geophysics*, vol. 72, no. 3, 2007, doi: 10.1190/1.2710183.

[12] S. Johnson, “Notes on Perfectly Matched Layers,” *Lect. notes, Massachusetts Inst*, no. August 2007, pp. 1–18, 2008.

[13] C. S. T. S. Suite, “CST Microwave Studio 2008 - Advertisement,” *IEEE Microw. Mag.*, vol. 8, no. 5, pp. 11–11, 2008, doi: 10.1109/mmw.2007.4383410

[14] D. Rhcp, “Series : Ceramic Patch Antenna PART NUMBER : W3229 • Applications requiring high gain directional antenna pattern Series : Ceramic Patch Antenna,” pp. 1–8, 1910.

[15] W. S. Chen, “Small circularly polarized microstrip antennas,” *IEEE Antennas Propag. Soc. Int. Symp. Wirel. Technol. Inf. Networks, APS 1999 - Held conjunction with Usn. Natl. Radio Sci. Meet.*, vol. 1, pp. 256–259, 1999, doi: 10.1109/APS.1999.789129.

[16] R. Selvaraju, M. H. Jamaluddin, M. R. Kamarudin, J. Nasir, and M. H. Dahri, “Complementary split ring resonator for isolation enhancement in 5G communication antenna array,” *Prog. Electromagn. Res. C*, vol. 83, no. January, pp. 217–228, 2018, doi: 10.2528/PIERC18011019.

[17] M. Gulam Nabi Alsath, M. Kanagasabai, and B. Balasubramanian, “Implementation of slotted meander-line resonators for isolation enhancement in microstrip patch antenna

arrays," *IEEE Antennas Wirel. Propag. Lett.*, vol. 12, pp. 15–18, 2013, doi: 10.1109/LAWP.2012.2237156.

[18] E. Engineering and U. T. Mara, "Mushroom-Like Electromagnetic Band Gap (Ebg)," no. 2, pp. 3–7.

[19] F. Yang and Y. Rahmat-Samii, "Microstrip Antennas Integrated with Electromagnetic Band-Gap (EBG) Structures: A Low Mutual Coupling Design for Array Applications," *IEEE Trans. Antennas Propag.*, vol. 51, no. 10 II, pp. 2936–2946, 2003, doi: 10.1109/TAP.2003.817983.

8. Appendices

8.1. MATLAB openEMS code

The final antenna design code did with MATLAB openEMS is presented below:

Setup the Simulation

```
physical_constants;
unit = 1e-3; % all length in mm
NumTS = 750000; %max. number of timesteps

% patch width in x-direction
patch.width  = 21; % resonant length
% patch length in y-direction
patch.length = 21;
% patch cut
patch.cut = 3.5;
% patch move
patch.move = 1.35;

% GroundPlane width in x-direction
gnd.width  = 70;
% GroundPlane length in y-direction
gnd.length = 70;

%substrate setup
substrate.epsR   = 7.75;
substrate.mue = 1;
substrate.width  = 25;
substrate.length = 25;
substrate.thickness = 4;
substrate.cells = 4;

% SMA dimensions
InnerDiameter = 0.8;      %pin diameter
OuterInnerDiameter = 0.8*2;     %outer diameter dielectric
OuterOuterDiameter = 0.8*2+0.075;    % outer diameter covering
CoaxLength = 2.01;          % length of coaxial connector
eps_teflon = 2.1;

%setup feeding
feed.pos = (-1)*((25/2)- 9.88); %feeding position in x-direction

% size of the simulation box
 SimBox = [200 200 150];
```

Setup FDTD parameters

```
f0 = 2.4e9; % center frequency
fc = 1e9;
f_start = f0-fc;
f_stop  = f0+fc;
```

```
freq = linspace(f_start,f_stop,201);
lambda = c0/(f0+fc);
```

Setup FDTD excitation function

```
FDTD = InitFDTD('NrTS',NumTS,'EndCriteria', 1e-5);
FDTD = SetGaussExcite(FDTD,f0,fc);

BC = {'PML_8','PML_8','PML_8','PML_8','PML_8','PML_8'};
FDTD = SetBoundaryCond(FDTD,BC);
```

Setup CSXCAD Geometry & Mesh

```
CSX = InitCSX();

%initialize the mesh with the "air-box" dimensions
mesh.x = [-SimBox(1)/2 SimBox(1)/2];
mesh.y = [-SimBox(2)/2 SimBox(2)/2];
mesh.z = [-SimBox(3)/3 SimBox(3)*2/3];
max_res = ceil(lambda/unit/50);

% Create Patch
CSX = AddMetal(CSX,'patch');
p(1,1) = -patch.width/2+patch.move;
p(2,1) = +patch.length/2 - patch.cut;
p(1,2) = -patch.width/2 + patch.cut+patch.move;
p(2,2) = +patch.length/2;
p(1,3) = +patch.width/2+patch.move;
p(2,3) = +patch.length/2;
p(1,4) = patch.width/2+patch.move;
p(2,4) = -patch.length/2 + patch.cut;
p(1,5) = patch.width/2-patch.cut+patch.move;
p(2,5) = -patch.length/2;
p(1,6) = -patch.width/2+patch.move;
p(2,6) = -patch.length/2;
CSX = AddPolygon(CSX,'patch',30,'z',substrate.thickness,p);

% Create Substrate
CSX = AddMaterial( CSX, 'substrate' );
CSX = SetMaterialProperty( CSX, 'substrate', 'Epsilon', substrate.epsR, 'Mue',
substrate.mue );
x=[-2 -1.9 -1.8:0.2:1.8 1.9 2];
y = sqrt (4-x.^2);
yNeg= -y;
vSize=12;
x1=x(1:vSize);
y1=y(1:vSize);
x2=x(vSize:(vSize*2)-1);
y2=y(vSize:(vSize*2)-1);
x3=x(1:vSize);
y3=yNeg(1:vSize);
x4=x(vSize:(vSize*2)-1);
y4=yNeg(vSize:(vSize*2)-1);
```

```
% Loop of polygon points
p = zeros(2,4*vSize);
   for j=1:vSize
       p(1,j) = x1(j)-substrate.width/2+2; p(2,j) = y1(j)+substrate.width/2-2;
       p(1,vSize+j) = x2(j)+substrate.width/2-2; p(2,vSize+j) = y2(j)+substrate.width/2-2;
       p(1,4*vSize+1-j) = x3(j)-substrate.width/2+2; p(2,4*vSize+1-j) = y3(j)-
substrate.width/2+2;
       p(1,3*vSize+1-j) = x4(j)+substrate.width/2-2; p(2,3*vSize+1-j) = y4(j)-
substrate.width/2+2;
   end
CSX = AddLinPoly( CSX, 'substrate', 1, 2, 0, p,substrate.thickness);

% Create Air Hole
CSX = AddMaterial( CSX, 'hole' );
CSX = SetMaterialProperty( CSX, 'hole', 'Epsilon', 1.00058986, 'Mue',1.0);
start = [feed.pos 0 0];
stop = [feed.pos 0 substrate.thickness];
CSX = AddCylinder(CSX, 'hole', 11, start, stop, InnerDiameter/2);

% add extra cells to discretize the substrate thickness
mesh.z = [linspace(0,substrate.thickness,substrate.cells+1) mesh.z];

% Create Ground
CSX = AddMetal( CSX, 'gnd' ); % create a perfect electric conductor (PEC)
start = [-gnd.width/2 -gnd.length/2 0];
stop  = [ gnd.width/2  gnd.length/2 0];
CSX = AddBox(CSX,'gnd',10,start,stop);

% Create Teflon dielectric
CSX = AddMaterial( CSX, 'teflon' );
CSX = SetMaterialProperty( CSX, 'teflon', 'Epsilon', eps_teflon);

% Create Coaxial Pin
CSX = AddMetal( CSX, 'metal' ); % create a perfect electric conductor (PEC)
start = [feed.pos 0 0];
stop = [feed.pos 0 substrate.thickness];
PinRad = InnerDiameter/2;
CSX = AddCylinder(CSX, 'metal', 15, start, stop, PinRad);

mesh = DetectEdges(CSX, mesh,'SetProperty','patch','2D_Metal_Edge_Res', lambda/unit/50);
mesh.x = SmoothMeshLines2( [mesh.x feed.pos-OuterOuterDiameter/2 feed.pos-
OuterInnerDiameter/2 feed.pos-InnerDiameter/2 feed.pos+InnerDiameter/2 ...
  feed.pos+OuterInnerDiameter/2 feed.pos+OuterOuterDiameter/2], max_res, 1.3);
mesh.y = SmoothMeshLines2([mesh.y -OuterOuterDiameter/2 -OuterInnerDiameter/2 -
InnerDiameter/2 InnerDiameter/2 OuterInnerDiameter/2 OuterOuterDiameter/2],max_res, 1.3);
mesh.z = SmoothMeshLines2([mesh.z -CoaxLength 0 substrate.thickness],max_res,1.3);

CSX = DefineRectGrid(CSX, unit, mesh);

% Coaxial and Port
start = [feed.pos 0 -CoaxLength];
stop  = [feed.pos 0 0];
[CSX,port] = AddCoaxialPort( CSX, 50, 1, 'metal', 'teflon', start, stop,
'z',InnerDiameter/2,OuterInnerDiameter/2,OuterOuterDiameter/2,'ExciteAmp',1);
```

```
% Dumb box
CSX = AddDump(CSX,'Et','FileType',1,'SubSampling','4,4,4');
start = [mesh.x(1)   mesh.y(1)   mesh.z(1)];
stop  = [mesh.x(end) mesh.y(end) mesh.z(end)];
CSX = AddBox(CSX,'Et',0 , start,stop);

% add a nf2ff calc box;
start=[mesh.x(12)     mesh.y(12)     mesh.z(12)];
stop=[mesh.x(end-11) mesh.y(end-11) mesh.z(end-11)];
[CSX nf2ff] = CreateNF2FFBox(CSX, 'nf2ff', start, stop);
```

Post-processing

```
postproc_only = 0;
openEMS_opts = '';
Settings = [];
Settings.LogFile = 'openEMS.log';
Sim_Path = 'tmp';
Sim_CSX = 'coax.xml';
if (postproc_only==0)
    [status, message, messageid] = rmdir(Sim_Path,'s');
    [status, message, messageid] = mkdir(Sim_Path);
end
```

Write openEMS compatible xml-file

```
if (postproc_only==0)
    WriteOpenEMS([Sim_Path '/' Sim_CSX],FDTD,CSX);
    CSXGeomPlot([Sim_Path '/' Sim_CSX]);
    RunOpenEMS(Sim_Path, Sim_CSX, openEMS_opts, Settings)
end
```

Postprocessing & Plots

```
port = calcPort(port, Sim_Path, freq);%,'RefImpedance', 50);
```

Smith chart port reflection

```
% feed point impedance plot
Zin = port.uf.tot ./ port.if.tot;
figure
plot( freq/1e6, real(Zin), 'k-', 'Linewidth', 2 );
hold on
grid on
plot( freq/1e6, imag(Zin), 'r--', 'Linewidth', 2 );
title( 'feed point impedance' );
xlabel( 'frequency f / MHz' );
ylabel( 'impedance Z_{in} / Ohm' );
legend( 'real', 'imag' );
```

```
% reflection coefficient S11 plot
s11 = port.uf.ref ./ port.uf.inc;
figure
plot( freq/1e6, 20*log10(abs(s11)), 'k-', 'Linewidth', 2 );
grid on
title( 'reflection coefficient S_{11}' );
xlabel( 'frequency f / MHz' );
ylabel( 'reflection coefficient |S_{11}|' );

drawnow

% Radiation patterns
f_res_ind = find(s11==min(s11));
f_res = freq(f_res_ind);

% calculate the far field at phi=0 degrees and at phi=90 degrees
disp( 'calculating far field at phi=[0 90] deg...' );
nf2ff_1 = CalcNF2FF(nf2ff, Sim_Path, f_res, [-180:2:180]*pi/180, [0 90]*pi/180,'Mode',1);

% display power and directivity
disp( ['radiated power: Prad = ' num2str(nf2ff_1.Prad) ' Watt']);
disp( ['directivity: Dmax = ' num2str(nf2ff_1.Dmax) ' (' num2str(10*log10(nf2ff_1.Dmax)) '
dBi)'] );
disp( ['efficiency: nu_rad = ' num2str(100*nf2ff_1.Prad./port.P_inc(f_res_ind)) ' %']);

% log-scale directivity plot
figure
plotFFdB(nf2ff_1,'xaxis','theta','param',[1 2]);

drawnow

% Show 3D pattern
disp( 'calculating 3D far field pattern and dumping to vtk (use Paraview to visualize)...'
);
thetaRange = (0:2:180);
phiRange = (0:2:360) - 180;
nf2ff_2 = CalcNF2FF(nf2ff, Sim_Path, f_res, thetaRange*pi/180,
phiRange*pi/180,'Verbose',1,'Outfile','3D_Pattern.h5');

figure
plotFF3D(nf2ff_2,'logscale',-20);

E_far_normalized = nf2ff_2.E_norm{1} / max(nf2ff_2.E_norm{1}(:)) * nf2ff_2.Dmax;
DumpFF2VTK([Sim_Path '/3D_Pattern.vtk'],E_far_normalized,thetaRange,phiRange,'scale',1e-
3);
```

The GPR antenna was designed copying the code above for the two antennas with the correct shift depending on the distance between Tx-antenna and Rx-antenna desired. Besides, for more information on the MATLAB openEMS codes used throughout this thesis, click on the following GitHub link:

https://github.com/albertnadal4/Bachelor-s-Thesis